Tectonics®

RESEARCH ARTICLE
10.1029/2024TC008660

# Kinematics and Age of the Orogen-Perpendicular Shkoder-Peja Normal Fault in North Albania Constrained by Fault-Slip Data, Raman Spectroscopy and K-Ar Fault-Gouge Dating

**Benjamin Schmitz[1], Peter Biermanns[2], Mathias Hueck[3,4], Klaus Wemmer[3], Stefan M. Schmid[5], Kujtim Onuzi[6], Klaus Reicherter[2], and Kamil Ustaszewski[1]**

[1]Friedrich-Schiller-Universität Jena, Institut für Geowissenschaften, Jena, Germany, [2]RWTH Aachen, Neotektonik und Georisiken, Aachen, Germany, [3]Georg-August Universität, Geowissenschaftliches Zentrum, Göttingen, Germany, [4]Ruhr-Universität Bochum, Institut für Geologie, Mineralogie und Geophysik, Universitätsstraße 150, Bochum, Germany, [5]Universität Basel, Departement Umweltwissenschaften, Basel, Switzerland, [6]Polytechnical University Tirana, Institute of Geosciences, Energy, Water and Environment, Tirana, Albania

**Key Points:**

- Post-Eocene brittle top-to-the SSE normal faulting along the Shkoder-Peja Normal Fault (SPNF) confirmed by detailed mapping and kinematic indicators
- Illite age analyses of fault gouges yielded Early Oligocene and Late Miocene ages for authigenic illite
- Post-Eocene SPNF activity is either continuous since early Oligocene or episodic with renewed (likely ongoing) extension since Miocene

**Supporting Information:**

Supporting Information may be found in the online version of this article.

**Correspondence to:**

B. Schmitz,
b.schmitz@uni-jena.de

**Citation:**

Schmitz, B., Biermanns, P., Hueck, M., Wemmer, K., Schmid, S. M., Onuzi, K., et al. (2025). Kinematics and age of the orogen-perpendicular Shkoder-Peja Normal Fault in north Albania constrained by fault-slip data, Raman spectroscopy and K-Ar fault-gouge dating. *Tectonics*, *44*, e2024TC008660. https://doi.org/10.1029/2024TC008660

Received 15 OCT 2024
Accepted 14 MAY 2025

**Author Contributions:**

**Conceptualization:** Kamil Ustaszewski
**Data curation:** Benjamin Schmitz, Klaus Wemmer
**Formal analysis:** Benjamin Schmitz, Mathias Hueck, Klaus Wemmer
**Funding acquisition:** Klaus Reicherter, Kamil Ustaszewski
**Investigation:** Benjamin Schmitz, Peter Biermanns, Mathias Hueck, Klaus Wemmer, Kamil Ustaszewski
**Methodology:** Benjamin Schmitz, Kamil Ustaszewski
**Project administration:** Kujtim Onuzi, Klaus Reicherter, Kamil Ustaszewski



**Abstract** The Shkoder-Peja Normal Fault (SPNF) is the largest orogen-perpendicular fault on the Balkan Peninsula, separating the Dinarides fold-and-thrust belt in the north from the Hellenides in the south. It has accommodated orogen-parallel extension during clockwise oroclinal bending of the Hellenic segment and juxtaposes Adriatic shelf successions in its footwall against obducted ophiolites in its hanging wall. Despite its length of at least 100 km, it is still an improperly understood fault. In this study, we combine results of geological mapping of a c. 13 km swath along the fault segment in Northern Albania with fault-slip data, Raman spectroscopy of carbonaceous matter (RSCM) and K-Ar dating of fault gouges to better constrain its kinematics and age. Our results provide evidence of top-to-the SSE extension across the SPNF, post-dating Eocene nappe stacking and truncating nappe-internal folds within the footwall. Illite crystallinity and RSCM data suggest that epizonal versus anchizonal conditions were reached in the footwall and hanging wall units, respectively. K-Ar dates of various grain size fractions (2–6, <2 and <0.2 μm) from fault gouges yielded ages between 47 and 106 Ma. Since these ages overlap with the minimum depositional ages of the stratigraphically youngest unit in the footwall, they are interpreted as mixed detrital and authigenic illite ages. Modeled ages for a pure authigenic illite fraction range between c. 34.4 and 6.2 Ma. As minimum temperatures of c. 100°C are required for the formation of authigenic illite, younger or even still ongoing fault activity at lower temperatures is likely.

**Plain Language Summary** The Shkoder-Peja Fault in northern Albania separates two mountain ranges: the Dinarides in the north and the Hellenides in the south. This study examines relative movements along this fault to better understand its history and significance for recent tectonic plate movements in the region by mapping and dating structures in the fault zone. By estimating the impact of heating of carbonaceous matter in sediments beneath the fault, we were able to determine that several km of rocks have been removed along the fault. Folds in the underlying rock formations were cut off during faulting and new clay minerals were formed along the interface, where the two rock formations slipped past each other. This clay mineral (illite) contains tiny amounts of a radioactive isotope ($^{40}$K) that was used for radiometric dating. Since the formation of this mineral requires temperatures above 100°C, the results indicate that the last movements along this section of the fault above this temperature occurred until some 6 Ma ago. Even younger deformation that occurred below this temperature (e.g., with less overburden) is to be expected; in fact, the fault could still be active today.

## 1. Introduction: Significance of the Shkoder-Peja Normal Fault

A recurring problem in characterizing past and present regional deformation patterns in many regions is constraining the timing of fault activity. Dating of fault activity is particularly important (a) if the studied faults are polyphase structures, (b) when their understanding is substantial to solve transregional geodynamical questions, and (c) when they occur in tectonically active areas. One such fault that satisfies all three criteria is the Shkoder-Peja Normal Fault (SPNF) on the central Balkan peninsula (Figures 1 and 2).

The SPNF is among the largest and most important orogen-perpendicular faults on the entire Balkan peninsula; it accommodated orogen-parallel extension in combination with large-scale clockwise rotations of crustal blocks

10.1029/2024TC008660

**Resources:** Kujtim Onuzi, Kamil Ustaszewski
**Software:** Benjamin Schmitz
**Supervision:** Kamil Ustaszewski
**Validation:** Peter Biermanns, Mathias Hueck, Klaus Wemmer
**Visualization:** Benjamin Schmitz, Stefan M. Schmid
**Writing – original draft:** Benjamin Schmitz
**Writing – review & editing:** Peter Biermanns, Mathias Hueck, Stefan M. Schmid, Kamil Ustaszewski

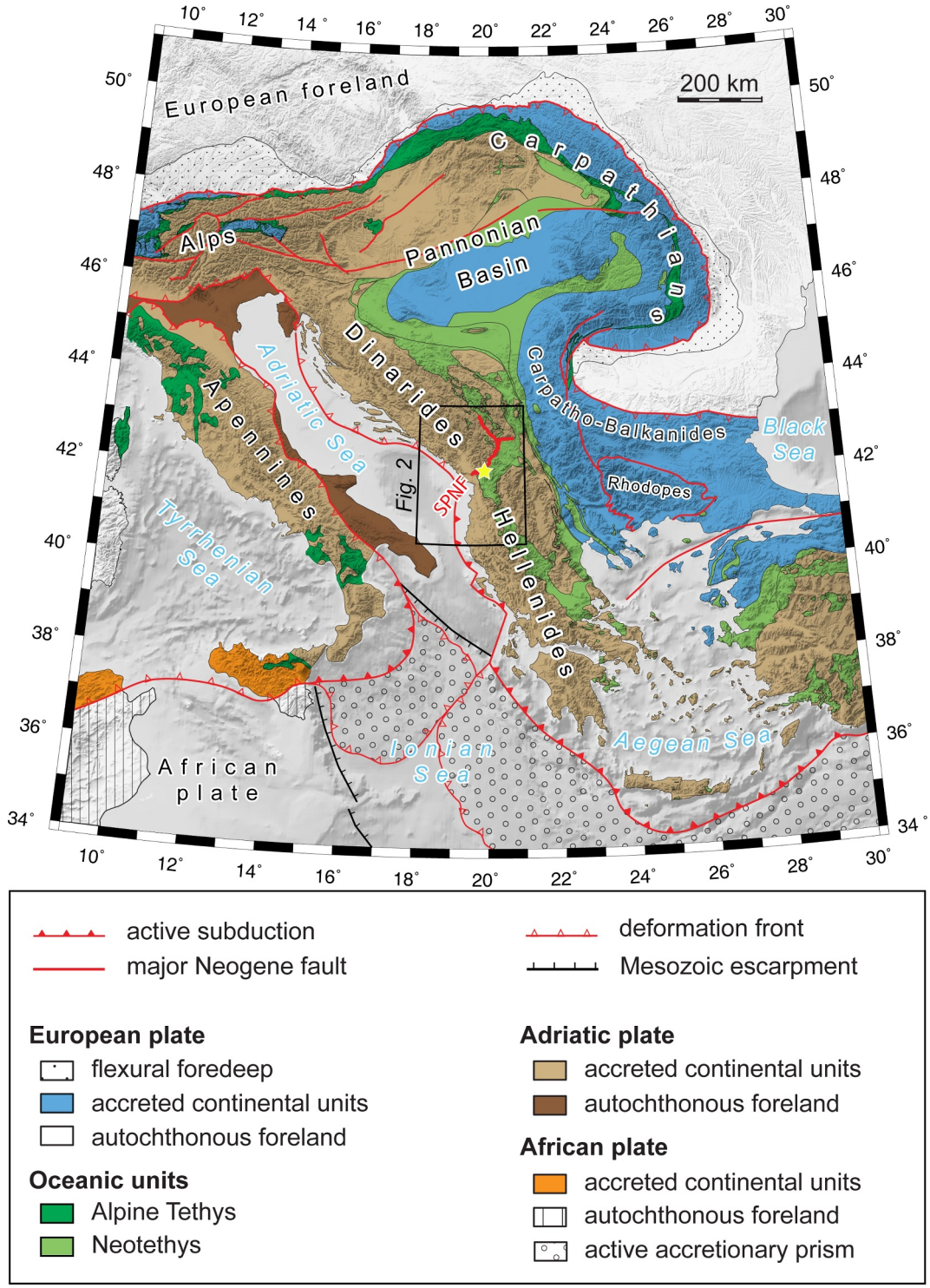


**Figure 1.** Alpine orogenic belts of the Africa-Europe convergence zone in the central Mediterranean. Colors correspond to the paleogeographic origin of the tectonic units (blue - accreted European and brown - Adriatic crust). Modified after Handy et al. (2019). The asterisk indicates the working area along the orogenic-scale Shkoder-Peja Fault which marks the transition from the Dinarides to the Hellenides, coinciding with a prominent bend in their general strike. SPNF = Shkoder-Peja Normal Fault.

10.1029/2024TC008660

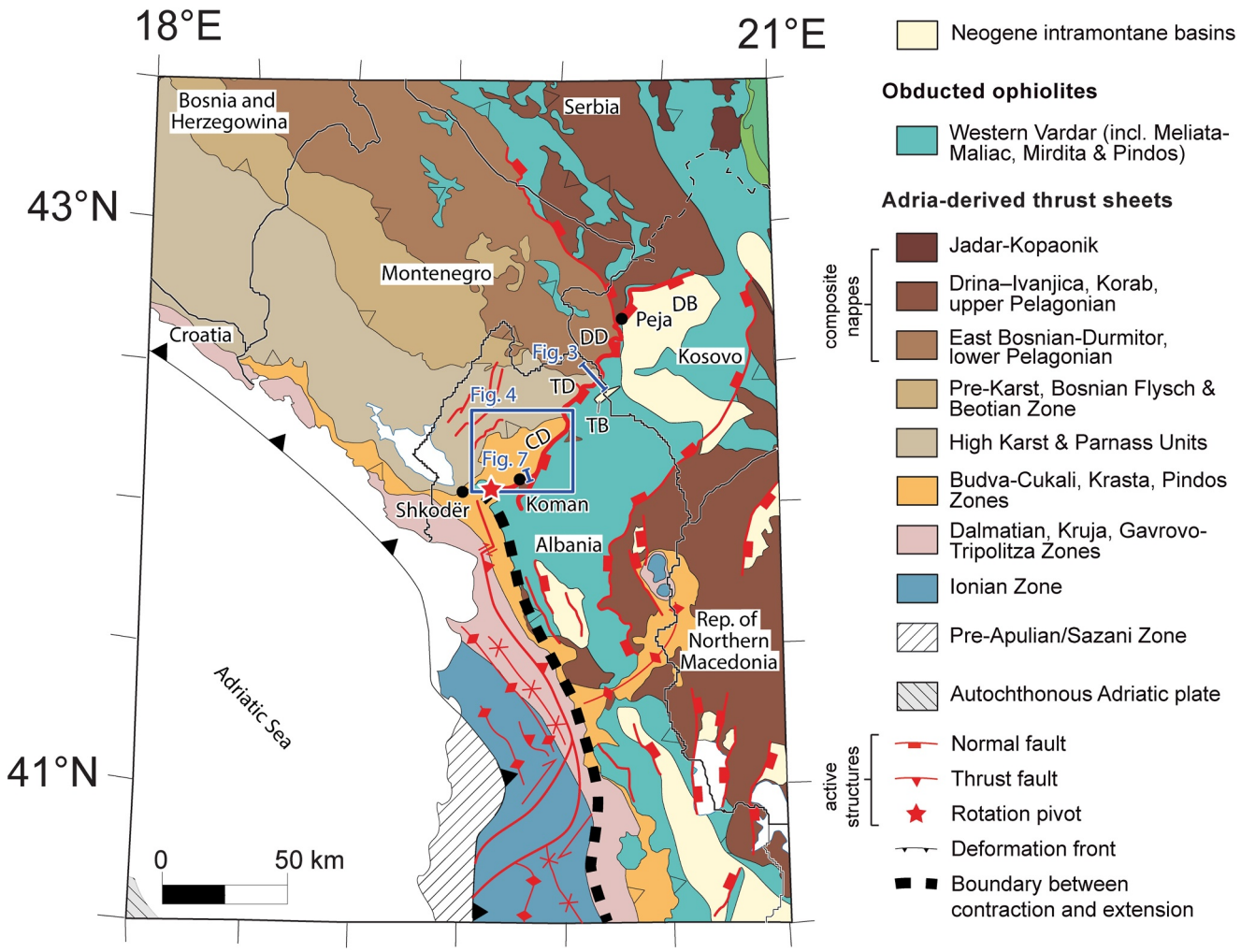


**Figure 2.** Geological overview map of the Albania-Montenegro border area modified after Schmid et al. (2008). Late Eocene to active faults and folds compiled from Dumurdzanov et al. (2005) and Handy et al. (2019). The working area is located at the southern rim of the Cukali Dome (CD) near Koman. TD = Tropoja Dome, DD = Dukagjini Dome, DB = Dukagjini Basin, TB = Tropoja Basin.

that accelerated in Neogene times (Handy et al., 2019; their Figure 11c). This rotation induced a change in the general trend of the otherwise topographically and tectonically continuous fold-and-thrust system of the Balkan peninsula into a northern NW–SE-trending segment, termed Dinarides, and a southern, NNW–SSE-trending segment, termed Hellenides (e.g., Schmid et al., 2020). Paleomagnetic studies suggest that the Hellenides experienced a post-Oligocene, clockwise rotation of in total some 45–50° (Kissel et al., 1995; van Hinsbergen et al., 2005; van Speranza et al., 1995) that is still ongoing (D'Agostino et al., 2020). The rotational pivot associated with normal faulting along the SPNF was placed near the town of Shkoder by Handy et al. (2019; see red asterisk in our Figure 2) while the rotation pole of the entire Dinarides-Hellenides orogenic system at a larger scale was placed more to the NW along the mid-Adriatic ridge offshore Dubrovnik (for more details see Handy et al., 2019). In contrast to these mostly Miocene to recent rotations no such paleomagnetic rotations in respect to stable Europe are known from the central and northern Dinarides since the Late Oligocene (Leeuw et al., 2012; Márton et al., 2016).

Activity of the SPNF is also associated with the formation of fault-bounded basins: Subsidence of the Dukagjini Basin in western Kosovo and in the Tropoja Basin in the northern Albania-Kosovo border area (DB and TB respectively in Figure 2) between the Mid-Miocene to Pliocene (c. 16 to 2.6 Ma) is linked to the activity of normal faulting along the SPNF (Handy et al., 2019).

Additional insight on the importance of the SPNF on a lithosphere-scale comes from seismic tomographic studies. Northwest of the SPNF, fast p-wave anomalies, interpreted as subducting lithospheric slabs, are hardly discernible below c. 100 km depth. This contrasts with the regions south of the SPNF, where the NW-ward extension of the NE-subducting Aegean slab can be imaged (Bijwaard & Spakman, 2000; Burchfiel et al., 2008; Handy et al., 2019; Jolivet et al., 2009; Koulakov et al., 2009; Serretti & Morelli, 2011). The SPNF hence appears to represent the surface expression of a lithosphere-scale bend or tear in the NE-ward subducting lithosphere underneath the Dinarides-Hellenides orogen (Handy et al., 2019). Its original detachment continued northwards to the SE Dinarides, where it connected with the Northern Montenegro Fault, Rožaje Fault, and Bjelasica Fault, enabling strain transfer and exhumation of mid-crustal rocks before it was cross-cut by secondary normal faults (Randjelovic et al., 2025). The kinematics of the SPNF, i.e., orogen-parallel extension in combination with clockwise rotation of the southern units, may be regarded as accommodating the decoupling of crustal units to either side of the fault. This decoupling is considered a consequence of the along-strike changes in the geometry of the slab underlying the stacked crustal units: The longer, untorn Hellenic segment accomplishes a faster rollback compared to the shorter Dinaric part of the slab (Handy et al., 2019). This in turn requires a corresponding structure in the upper crust in the transition area, which facilitates different rollback rates. It is believed that the SPNF plays an important role in this process, making it a fundamental lithosphere-scale feature that governs the kinematic and structural evolution of the entire orogenic junction. Its location roughly coincides with the southern limit of post-collisional mantle delamination beneath the Dinarides, which resulted in a Late Oligocene-Miocene uplift of marine terraces of up to 600 m asl (Balling, Grützner, et al., 2021). Previous studies postulated that the normal faulting activity along the SPNF followed a pre-existing zone of weakness, a Jurassic rift transfer in the West Vardar Ocean (Aubouin & Dercourt, 1975; Bernoulli & Laubscher, 1972; Handy et al., 2019). Because of the fact that in present time map view the front of the Western Vardar ophiolites is dextrally offset by some 80 km (Schmid et al., 2020), as shown in Figure 2, most of this offset must pre-date normal faulting along the SPNF. Substantial components of this dextral large offset may have occurred during Late Eocene closing of the hemipelagic Krasta-Cukali deep-water basin or even earlier and during the latest Jurassic obduction of the West Vardar ophiolites (see discussion in Schmid et al., 2020; their page 347). In any case, normal faulting along the SPNF post-dates folding and thrusting of the Krasta-Cukali Unit, which ceased after the Early Oligocene, coinciding with the onset of the above-mentioned uplift of undeformed marine terraces along the Dinaric coast (Balling, Grützner, et al., 2021). The question after the Pliocene to recent activity of the SPNF remains largely uncertain. However, the eastern, N–S striking splay faults of the SPNF, which are bordering the western Dukagjini Basin (Kosovo) show geomorphological evidence of recent E–W extension such as narrow wineglass-shaped valleys and triangular facets (D'Agostino et al., 2022). Furthermore, geodetic measurements based on GNSS (Global Navigation Satellite System) carried out in addition to these observations also give reason to believe that the fault activity in areas adjacent to the SPNF has not ceased yet (D'Agostino et al., 2020, 2022; Jouanne et al., 2012).

This study uses a multidisciplinary approach to understand the kinematic evolution and timing of brittle faulting along the westernmost segment of the SPNF in northern Albania. The approach integrates structural mapping and geochronology to elucidate its deformation history: structural mapping provides an understanding of the relative timing between folding and faulting along the central southern Krasta-Cukali Dome by describing cross-cutting relationships and fault-slip vectors. Raman spectroscopy of carbonaceous matter (RSCM) and illite crystallinity were employed to quantify peak metamorphic temperatures in footwall units and within the fault zone respectively, which constrain the thermal conditions during faulting and allow an estimate for the vertical offset. K-Ar dating of illite in fault gouges provides temporal constraints on brittle fault activity. In combination with illite age analysis (IAA), which is used to distinguish the fractions of authigenic (synkinematic) versus detrital illite by quantifying its polytypes ($1M/1M_d$ vs. $2M_1$, respectively), these techniques provide a better understanding of brittle faulting in the temperature range where illite growth is expected.

## 2. Geological Setting

The research area is located within the continent-continent collision zone between Adria and Eurasia in northern Albania (Figures 1 and 2). The emplacement of SW-vergent, Adria-derived thrust sheets largely occurred between the Late Cretaceous and the Oligocene and built up the fold-and-thrust belts of the Dinarides and Hellenides (Schmid et al., 2008). However, south of the SPNF, i.e., in the Hellenides, a younger, mostly post-Mid Miocene phase of shortening and nappe stacking phase is documented that partly reactivated earlier thrusts (Handy

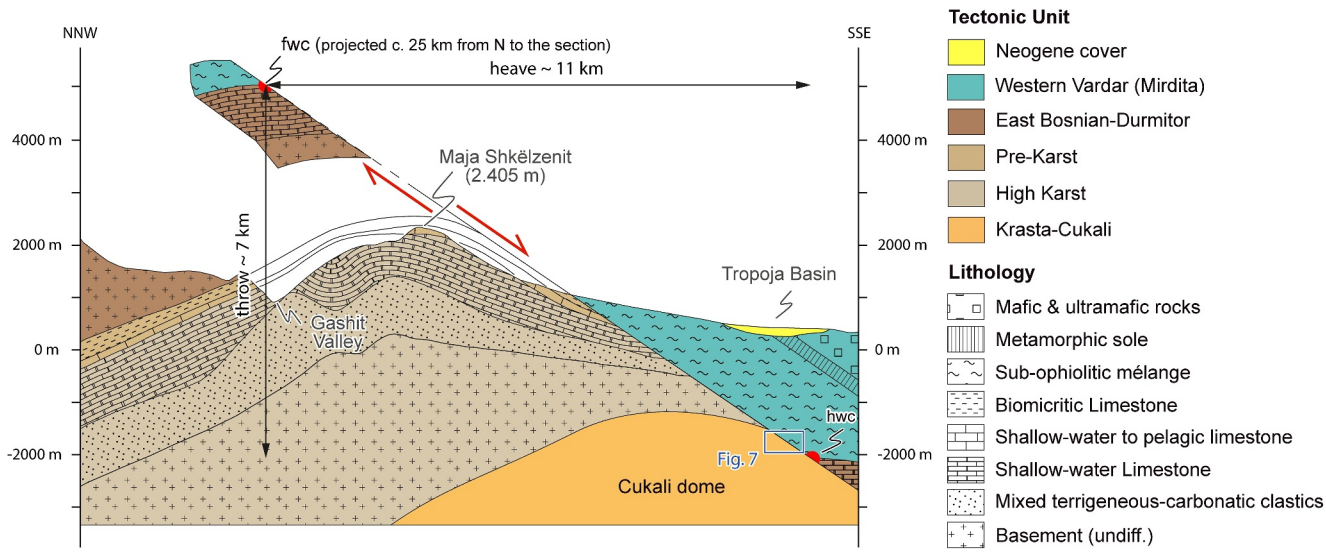


**Figure 3.** Cross section through the Shkoder-Peja Normal Fault near Bajram Curri, easternmost Albania, modified after Handy et al. (2019). Here, the vertical throw of the hanging wall (Mirdita/West Vardar Unit) compared to the footwall (High Karst/Albanian Alps Unit) amounts to 7 km while at the south-westernmost edge of the Cukali Dome no offset is distinguishable. The reference contact (Mirdita/West Vardar Unit on East Bosnian Durmitor Unit) in the footwall was projected into the profile about 25 km from the nappe outlier to the north. fwc = footwall cutoff, hwc = hanging wall cutoff. See Figure 2 for localization of the cross section.

et al., 2019). Dinarides and Hellenides alike are structurally divided into internal and external units. In contrast to the external units, the internal units represent composite nappes comprising continental deposits of the Adria passive margin as well as previously obducted ophiolites. Obduction onto the distal Adriatic passive margin already occurred in the Late Jurassic (Aubouin et al., 1970; Schefer et al., 2010; Sudar & Kovács, 2006). Both the ophiolitic and underlying passive margin successions were subsequently involved into continent-continent collision since the Late Cretaceous (Pamić, 1993, 2002; Schmid et al., 2008; Tari & Pamić, 1998; Ustaszewski et al., 2009). The external units consist mainly of Mesozoic to Paleogene shallow marine carbonate rocks derived from the eastern Adriatic carbonate platform (Schmid et al., 2008). These units underwent thin-skinned deformation with SW-propagating thrusting toward the Adriatic foreland during the Mid-Eocene to Oligocene north of the SPNF in the Dinarides (Balling et al., 2023), and WSW-propagating ongoing thrusting since the Late Eocene south of the SPNF in the Hellenides (Aliaj et al., 2001; Papanikolaou, 2013).

The structural transition between the NW-SE striking Dinarides and the NNW-SSE striking Hellenides coincides with the location of the above described major orogen-perpendicular fault between the cities of Shkoder (northern Albania) and Peja (western Kosovo). At present, this orogen-perpendicular "Shkoder-Peja Fault" represents a SE-dipping normal fault separating mostly oceanic units of the Mirdita ophiolite (a part of the West-Vardar ophiolites sensu Schmid et al., 2020) in the hanging wall from pelagic Mesozoic to Palaeogene successions of the Cukali window in its footwall (Figures 3 and 4).

Associated with the clockwise rotation of the southern Balkan peninsula is a differential vertical throw along-strike the SPNF. The throw is negligible around Shkoder, but increases to around 7 km near the border between Albania and Kosovo (Figure 3) (Handy et al., 2019). We mapped a 3 km wide and 13 km long corridor along the southern rim of the Cukali Dome—mainly in the footwall of the Cukali-Tropoja Fault in great detail (Figure 4b). The Cukali Dome forms a NE–SW-trending halfwindow with a maximum length and width of c. 50 × 30 km, exposing dominantly pelagic to hemipelagic successions of the Krasta-Cukali Unit. In detail, it encompasses a sedimentary succession of Triassic volcanoclastics and neritic limestones followed by Jurassic shales, radiolarian cherts and calcareous turbidites, Cretaceous pelagic limestones and Paleocene-Eocene siliciclastic turbidites and marls (Robertson & Shallo, 2000).

The Krasta-Cukali Unit is juxtaposed against the ophiolitic West Vardar/Mirdita Unit in the south along the SE-dipping SPNF. Internally, the NE-SW-trending Cukali halfwindow reveals a set of narrow NW-SE-to E-W-striking folds with average spacings of c. 1–5 km (Figure 4). Along the northwestern margin of the Cukali Dome, the successions are overthrust by the Albanian Alps Unit in the NW (referred to as High Karst Unit in former

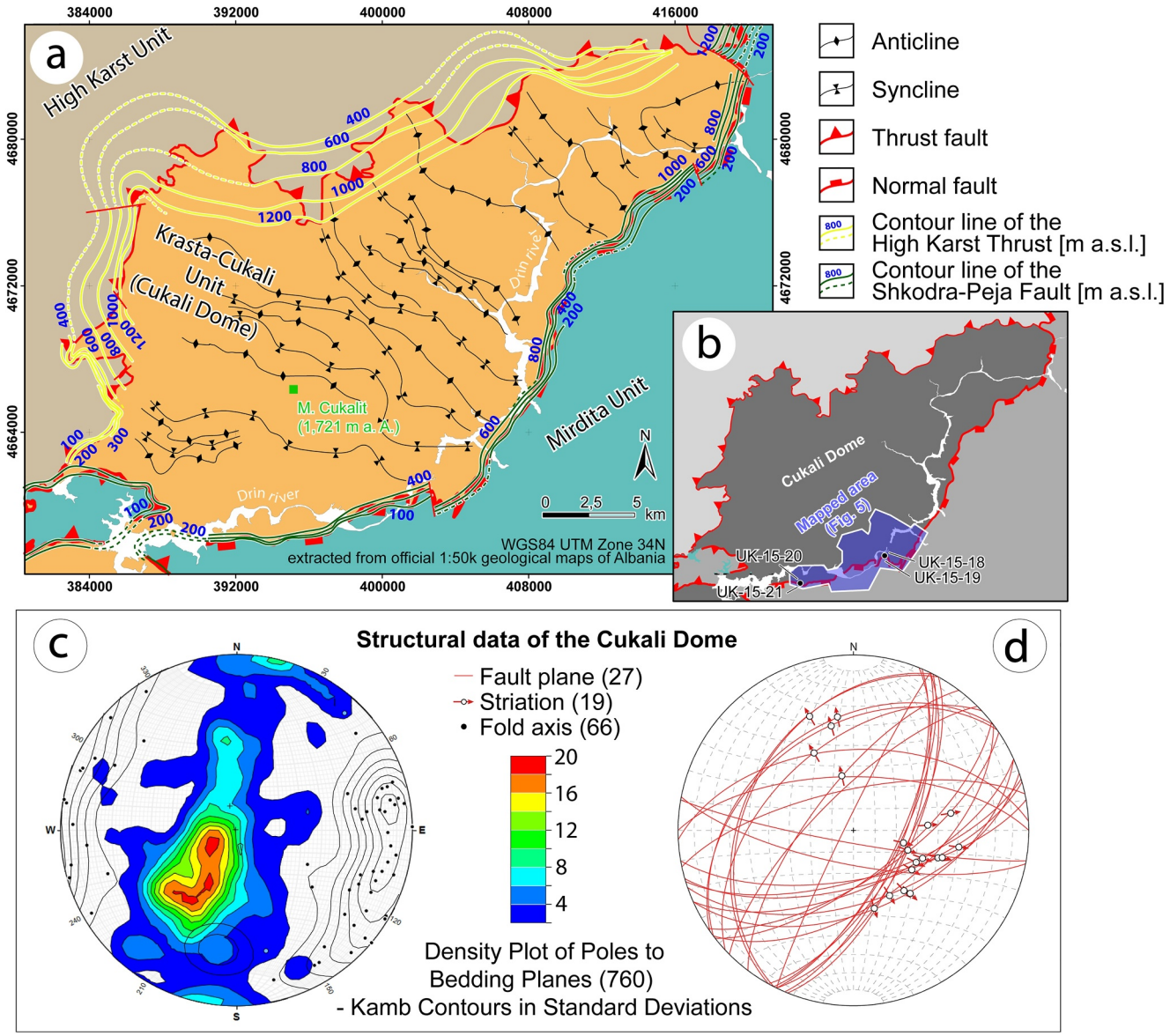


**Figure 4.** (a) Structural map of the Cukali Dome, modified after Cionoiu et al. (2014). Internal folds strike predominantly NW–SE but turn into an E-W strike in the working area. (b) Localization of the study area and sampling sites for K-Ar dating of fault gouges. (c) Structural data of the (Krasta-)Cukali Unit. Mean orientation of the fold axis is 105/10 (plunge direction, plunge angle). (d) Fault-slip data along the Shkoder-Peja Normal Fault showing a consistent normal faulting regime. Stereoplots were constructed using the open source software Stereonet and Innstereo.

Yugoslavia; see Schmid et al. (2020) for an exhaustive comparison of the terminology of tectonic units adopted in the Dinarides and Hellenides). The NW-SE striking large-scale (km) folds are predominantly upright in the NE and show increasing SW- to S-vergence toward the SW (Meço & Aliaj, 2000). In the southern part of the half-window, the folds strike E-W (Figure 4a).

## 3. Methods and Rationale

Our field investigations included geological mapping of c. 50 km$^2$ at a scale of 1:10,000 (Figure 5) along a c. 13 km long central section of the southern edge of the Cukali-Halfwindow to both sides and along-strike of the SPNF (for the location see Figure 4b). The rationale for this approach was to cast more light onto the geometry and kinematics of the SPNF along a relatively easily accessible segment between Shkoder and Koman (Figure 2). Along this fault, we sampled fault gouges for potassium-argon (K-Ar) dating to determine ages of newly formed

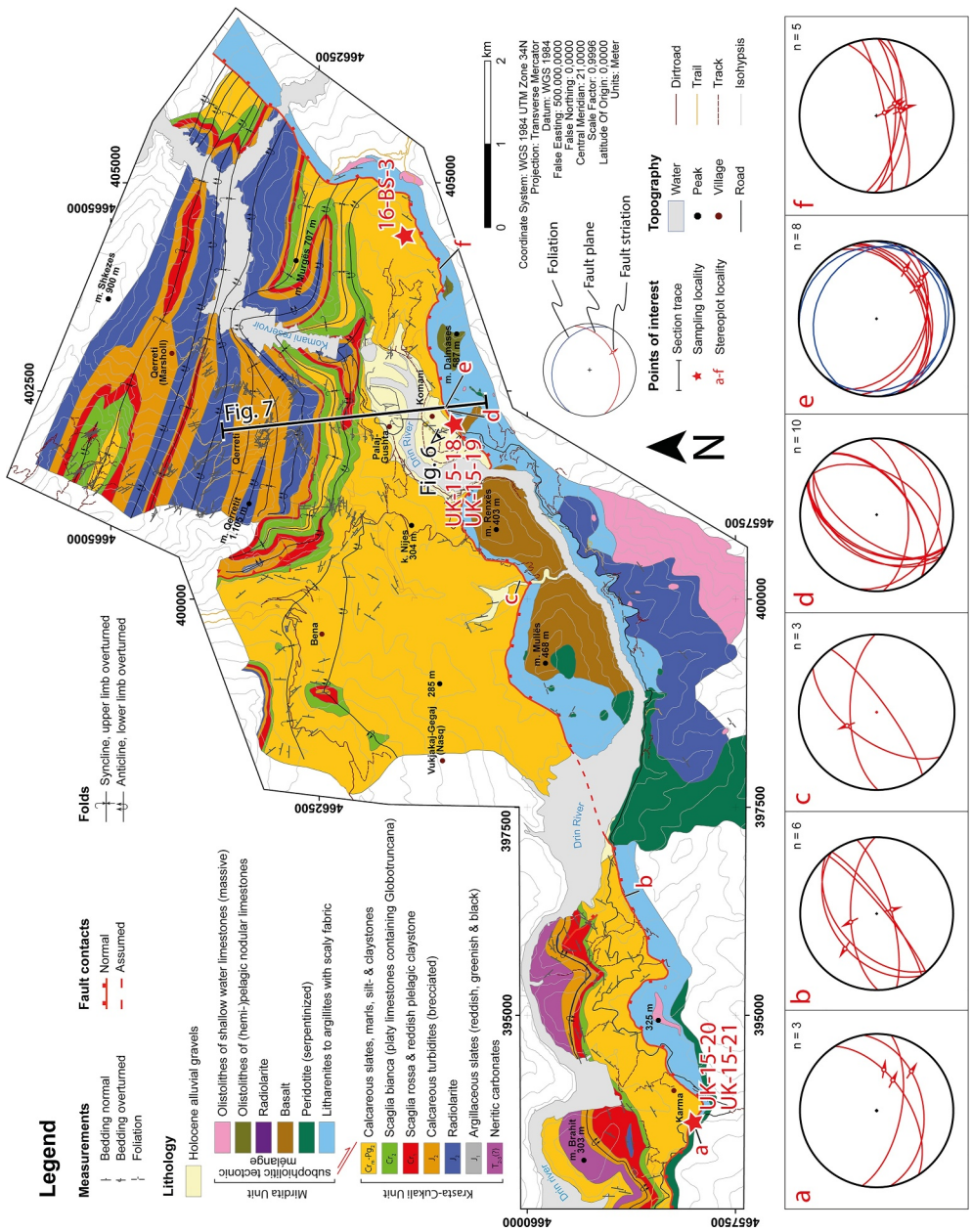


**Figure 5.** Detailed geological map of the southern Cukali Dome adjacent to the Shkoder-Peja Normal Fault (SPNF) with the distinction of several lithostratigraphic units. Mesozoic pelagic successions to Eocene calcareous slates and siliciclastics are involved into km-scale south-vergent thrust-related folds and truncated by the top-to-the SSE-directed SPNF. The hanging wall encompasses a sub-ophiolitic tectonic block-in-matrix mélange (sensu Festa et al., 2019) with exotic blocks of serpentinized peridotite, basaltic rocks and olistholiths of radiolarites, and limestones. See online supplementary for an enlarged, high-resolution version of this figure. (a)–(f) Stereoplots of fault-slip data along the SPNF. All measurements indicate NW-SE directed extension. (a) Normal faulting at sampling site UK-15-20 and UK-15-21. (b) Conjugated normal faults in the hanging wall. (c) Small-scale conjugated normal faults offsetting a sandstone layer in the footwall. (d) Conjugated normal faults in the footwall and (e) SC-fabrics (blue and red great circles respectively) indicating top-to-the SE directed normal faulting in the hanging wall, both at sampling site UK-15-18 and UK-15-19. (f) Top-to-the SSE directed normal faulting in the footwall close to sampling site 16-BS-3. Stereoplots were constructed using the open source software Innstereo.

**Table 1**
*List of Sampling Locations Along the Shkoder-Peja Normal Fault With Coordinates, Information About the Fault Gouge Lithology and Structural Position*

| Method | Sample name | Structural Position | Coordinates | Locality |
|---|---|---|---|---|
| K-Ar and IC | UK-15-18 | lower position within fault zone (footwall lithology) | UTM 34T 402154/4660903 | S of Koman, near to the intersection of the SH25 road and incised gully Përroi Grazhdës |
| | UK-15-19 | higher position within fault zone (hanging wall lithology) | | |
| | UK-15-20 | lower position within fault zone (footwall lithology) | UTM 34T 393756/4657996 | Approximately 9 km WSW of the first sampling location on the western side of the gully near the village Markolaj (Karmë) |
| | UK-15-21 | higher position within fault zone (hanging wall lithology) | | |
| RSCM | 16-BS-3 | Footwall | UTM 34T 404661/4661413 | c. 2,5 km E of Koman on the gravel road to the peak of the hill Maja Les |

illite. Fault gouges are non-cohesive fine-grained, clay-rich rocks formed in the frictional regime by fracturing and abrasive wear in brittle fault zones, involving grain comminution (Fettes & Desmons, 2007; Heitzmann, 1987; Sibson, 1977, 1986), usually at shallow-crustal conditions below c. 100°C (Fossen & Cavalcante, 2017). Numerous case studies have convincingly demonstrated the feasibility of dating fault gouges by means of the K-Ar technique to deduce ages of faulting in a temperature range below the frictional-viscous transition (Hueck et al., 2020; Kralik et al., 1987; Tsukamoto et al., 2020; Vrolijk et al., 2018; Zwingmann & Mancktelow, 2004; Zwingmann et al., 2010). The feasibility of K-Ar dating of fault gouges containing clay minerals (in contrast to merely clay-sized mineral fragments) relies on the growth of newly formed, authigenic K-bearing phases (such as illite) that are kinematically linked to brittle faulting events. For dating newly formed illite fractions, minimum temperature conditions of c. 100°C must be met (Pleuger et al., 2012). Below that temperature, it is increasingly likely that only mineral components inherited from the wall rock will be dated, which are genetically unlinked to the tectonic event creating the gouges in which they are contained.

In order to better understand our K-Ar results and the thermal maturity attained by our sample material, we also performed illite crystallinity analysis (IC) on the same samples and, additionally, Raman spectroscopy of carbonaceous matter (RSCM) within siliciclastic successions from the footwall. K-Ar analyses were complemented by Illite age analyses (IAA), using different illite polytypes ($2M_1$ vs. $1M/1M_d$), to differentiate between inherited and authigenic illite fractions and extrapolate authigenic end-member ages in our dated samples (e.g., van der Pluijm et al., 2001).

### 3.1. Sampling Sites

Fault gouges were sampled for K-Ar dating at two sites along a segment of the SPNF that was previously mapped in detail (Figure 5). The sampling sites are separated by approximately 8 km along strike and were selected based on outcrop accessibility and minimum width of the fault zone. This is particularly important when sampling fault gouge from an anastomosing fault, where slip may have repeatedly shifted between different strands within a wider fault zone over time. Both sampling sites are located close to the road between the villages of Karma and Koman (Figure 5 and Table 1). At each site, two aliquots of fault gouge were sampled within the core zone of the fault after removal of a thickness of c. 10–20 cm of surface material (vegetation, soil, weathered material and occasionally slope scree). We sampled gouges hosted in lithologies derived from both the footwall as well as the hanging wall of the SPNF. The idea of assigning the samples to footwall and hanging wall lithologies resulted from the strong tectonisation of the fault zone: Sometimes the anastomosing fault branches contained coherent gouges, which were better developed in one lithology, and sometimes better in the other lithology, but never in the direct contact zone. The distinction between footwall and hanging wall lithologies in the field was based on differences in color and carbonate content of the involved rocks. Calcareous and bright-colored clayey gouge was attributed to strongly tectonized Paleocene to Eocene slates and marls of the Cukali Unit in the footwall (Figure 6). Dark gray to blackish, non-calcareous, often more indurated gouge was considered to be derived from litharenites to non-calcareous slates commonly found in the matrix of the subophiolitic mélange, exposed in the hanging wall of the SPNF (Figure 6). This approach was driven by the observation that non-cohesive, purely

10.1029/2024TC008660

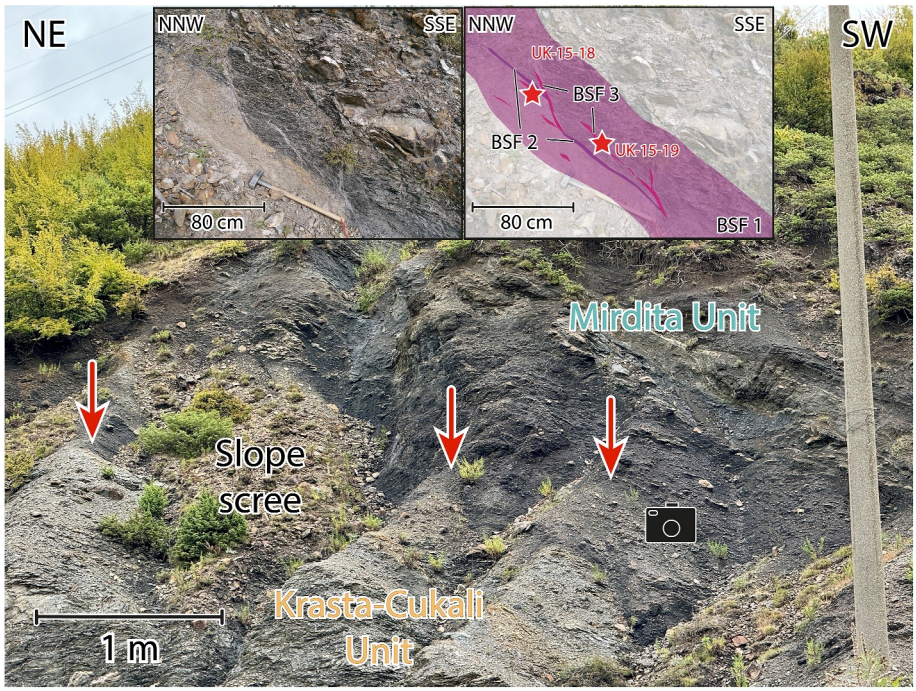


**Figure 6.** Sampling site of UK-15-18 and UK-15-19 south of Koman (red asterisks in the inset, see also Figure 12a). Camera symbol indicates the area of the detailed inset photography and its interpretation of Brittle Structural Facies sensu Tartaglia et al. (2020), for further information see Section 5.1. The outcrop exhibits the fault core and parts of the damage zones of the Shkoder-Peja Normal Fault. The Krasta-Cukali Unit (footwall) with its strongly tectonized Paleocene to Eocene slates and marls is calcareous and appears lighter in color. The strongly tectonized litharenites to slates of the Mirdita Unit with its subophiolitic mélange of supposed Jurassic age in the hanging wall appear much darker and are non-calcareous. Red arrows trace the color change between footwall and hanging wall.

clayey gouge along the fault was never encountered in thicknesses greater than a few centimeters, so that all gouge samples also included strongly tectonized, weakly indurated lithic fragments.

Additionally, three samples of coal-rich lithic sandstone of Paleocene-Eocene age in the footwall were taken for Raman spectroscopy of carbonaceous matter (RSCM). The outcrop is located in a road cut along a gravel road leading from Koman to the top of the hill Maja Les in the easternmost parts of the mapped area in the footwall of the SPNF, structurally c. 20 m below the fault zone (16-BS-3 a-c; Table 1). The medium-grained sandstone shows a calcitic cement and contains coal chippings very likely derived from terrestrial plants of up to $2 \times 2 \times 0.1$ cm.

### 3.2. Thermal Evolution and Metamorphic Grade of the Central Shkoder-Peja-Normal-Fault-Zone

During brittle faulting, the formation of authigenic sheet silicates such as illite can accompany the formation of fault gouges by grain comminution formed by abrasive wear during frictional deformation (van der Pluijm et al., 2001; Vrolijk & van der Pluijm, 1999). The restructuration of illite into different polytypes is used to quantify possible mixing between clay-sized white mica inherited from the wall rock and authigenic illite (see review in Hueck et al., 2022): The stable $2M_1$ polytype is dominant above temperatures of 280°C (Velde, 1965) and can be considered the inherited component, whereas the $1M/1M_d$ polytype is dominant in the typical temperature regime of shallow crustal faults below 150°C (Grathoff et al., 2001; Tsukamoto et al., 2020; van der Pluijm et al., 2001; Vrolijk et al., 2018). Therefore, the formation of authigenic illite ($1M/1M_d$) within the fault gouge can be correlated with fault activity (Kralik et al., 1987; Lyons & Snellenburg, 1971). The illite crystallinity index (Kübler, 1967) is a temperature-dependent empirical measurement that is used to estimate the peak metamorphic grade during illite formation based on the increasing crystallographic ordering and decreasing lattice strain, resulting in coarsening crystallite thickness (Moore & Reynolds, 1997; Warr, 2018). To confirm the estimated temperature range and to determine the overburden, three samples were taken from the topmost footwall lithologies for peak metamorphic temperature assessment by RSCM. Key methodological information is

provided in the following sub-sections. A more detailed description of the analytical setups is given in the Text S2 in Supporting Information S1.

#### 3.2.1. Illite Crystallinity

Illite crystallinity, quantified by the Kübler Index (KI), which represents the full width at half maximum of the 001 XRD reflection, was calculated to estimate the diagenetic to low-grade metamorphic conditions during illite formation. Samples were measured in the air-dried and glycolyzed state to access the smectite fraction within the illite-smectite interlayers (I/S). The mineralogy and illite crystallinity were determined by X-ray diffraction on a glass slide in a Phillips PW 1800 X-ray diffractometer. Inter-laboratorial calibration was performed using the Crystallinity Index Standards (CIS) following the recommendations of Warr and Rice (1994) and Warr (2018), as described in Hueck et al. (2022) and afterward recalculated from the CIS scale to the KI using the equation from Warr and Ferreiro Mählmann (2015). In the subsequent text, the illite crystallinity is only given and discussed in the converted Kübler values.

#### 3.2.2. Raman Spectroscopy of Carbonaceous Matter

To confirm the results of illite crystallinity and to determine an absolute temperature range caused by the sedimentary and/or tectonic overburden, organic-rich Paleocene-Eocene litharenite of the footwall were sampled to perform RSCM. Paleotemperature was calculated using the thermometers of Lahfid et al. (2010) following the procedures described in the Text S3 in Supporting Information S1. Measured spots were classified into three quality levels from 3 (poor) to 1 (very good) according to their location within the carbonaceous matter, masking by other minerals, subjective degree of weathering, intensity of the background signal and the signal-noise-ratio.

### 3.3. K-Ar Dating and Illite Age Analysis of Illite-Rich Fault Gouges

To constrain the age of brittle faulting below c. 150°C along the SPNF, illite-rich fault gouge samples (see Section 3.1) were dated using the K-Ar method. Isotopic analyses of three grain size fraction samples (<0.2 μm, <2 μm and 2–6 μm) were carried out at the University of Göttingen, Germany. Potassium content was determined by flame photometry (BWB-XP from THG-Glock Instruments), while the argon isotopic composition was determined by mass spectrometry (ARGUS VI from Thermo Scientific) after isotope dilution according to procedures described by Wemmer (1991) and Löbens et al. (2011). To compute pure authigenic ages uncontaminated by inherited mineral fragments (i.e., 100% 1M/1$M_d$ Polytype, 0% 2$M_d$ polytype, quantified following the peak-comparison method of Grathoff and Moore (1996) with current application described in Hueck et al., 2022), IAA was performed as a two-endmember mixing model (e.g., van der Pluijm et al., 2001).

## 4. Results and Interpretation

### 4.1. Description of the Mapped Geological Units

In total, we distinguished 13 mapping units based on lithostratigraphic criteria (Figure 5). Lithologies of the Krasta-Cukali Unit in the footwall of the SPNF are juxtaposed against lithologies attributed to the Mirdita Unit forming its hanging wall. The lowermost lithostratigraphic units of the Krasta-Cukali Unit exposed in our study area are represented by Middle to Late Triassic neritic limestones. These are covered by a pelagic succession of platy limestones and slates, leading to the sedimentation of Early Jurassic pelagic limestones of Ammonitico Rosso facies and grainstones to conglomeratic breccias. Middle to Late Jurassic alternations of stratified pelagic limestones are followed by a transition into turbiditic calcarenites, litharenites and argillaceous rocks deposited around the Jurassic-Cretaceous boundary. Calcarenites and litharenites contain submarine slump horizons. Toward the end of the Late Cretaceous, platy, Globotruncana-bearing limestones give way to Maastrichtian to Eocene terrigenous turbiditic deposits dominated by alterations of calcareous slates, marls, silt- and claystones with local occurrences of decimeter-thick slump horizons.

The Mirdita Unit in the mapped area encompasses a subophiolitic, block-in-matrix-type tectonic mélange (Festa et al., 2019; Gawlick & Missoni, 2019) with blocks of serpentinized peridotite, basaltic rocks, radiolarite as well as olistholiths of massive shallow water limestone and (hemi-)pelagic nodular limestones of unknown age in an argillaceous slaty matrix revealing scaly (i.e., post-depositional, tectonic) fabrics. This tectonic mélange underlies

the obducted ophiolitic units (Figure 3) and formed during latest Jurassic to earliest Cretaceous obduction (Kimmeridgian or later; Gerzina & Djeric, 2016; Schmid et al., 2020; Vishnevskaya et al., 2009).

### 4.2. Newly Identified Structures and Fault Kinematics Around the SPNF

In the mapped area, lithologies of the Krasta-Cukali Unit are all incorporated into km-scale south-vergent folds related to Eocene to Early Oligocene shortening during the Dinaric phase (Balling, Tomljenović, et al., 2021; Schmid et al., 2020). The axial planes dip c. 30–60° toward NNE (Figure 7) with a slight plunge of the fold axes to ESE (Figure 4c). Lithologies susceptible to folding (such as radiolarites and slates) developed tight to isoclinal small-scale folds (Figures 7c and 7d). All folds, regardless of their scale and orientation, are equally truncated by the SPNF along the southern edge of the halfwindow (Figures 5, 7, and 8 and Figure S5 in Supporting Information S1). This observation constrains the maximum age of the onset of normal faulting along the SPNF to post-Eocene times, based on the stratigraphic age (Eocene) of the youngest lithostratigraphic unit crosscut by the SPNF. Throughout the entire mapped length of the SPNF, the fault zone manifests itself as a c. 0,52 m thick core (Figure 7f) encompassed by an at least 10–20 m wide damage zone, which separates the ophiolitic Mirdita Unit (hanging wall) from the folded pelagic succession of the Krasta-Cukali Unit (footwall, Figures 6 and 7). The fault core exhibits a foliated fabric with several, partly diffuse fault strands instead of a single distinct plane. Kinematic indicators like S-C fabrics show top-to-the S to SSE-directed shear (Figures 5e, 12a, 12b, 12e, and 12f). In combination with conjugate normal faults (Figures 5b–5d), this consistently indicates deformation in a normal faulting regime (Figure 7f) associated with NNW–SSE extension.

### 4.3. Estimates of Paleotemperature Conditions, Overburden, and Slip Rates Along the SPNF

The occurrence of abundant Class 2 to Class 3 similar folds (see cross section in Figure 7 and field pictures Figures 7a, 7e, and 8b) with thickened fold hinges next to thinned fold limbs (Ramsay, 1967) and pervasive development of axial plane cleavages in lithologies prone to pressure solution (limestones, marls, slates; see Figures 7a and 7e) suggest at least upper diagenetic to lower anchizonal conditions during pre-SPNF south vergent deformation in the footwall. Thermometers 1 and 2 after Lahfid et al. (2010) were applied to 3 samples with suitable lithologies from the eastern mapping area (16-BS-3 a–c) and yielded an average peak temperature of 219 ± 50°C and 217 ± 48°C, respectively (Figure 9).

Weighting according to the quality levels explained in Section 3.2.2 did not lead to any significant change in the results (216°C and 214°C, respectively). Both, quality-weighted and unweighted paleotemperature estimates are consistent with a recently published study of Grund (2023) that interpolated the RSCM-based peak temperature regime in the external Dinaric nappes in northern Albania and Kosovo from 180°C close to Shkoder to 280°C close to Bajram Curri. Assuming an average continental geothermal gradient of 30°C/km, our estimated peak temperatures of 215°C would correspond to an overburden of about 7.2 km, which is also in agreement with a geometrically constrained reconstruction of about 7.0 km in a profile near Bajram Curri (Figure 3, see also Handy et al., 2019). Assuming a post-Eocene onset of normal faulting at constant slip rates along the SPNF (dipping at 35° toward S) and disregarding erosional unroofing, the tectonic removal of about 7.2 km of overburden (as estimated from the approach above) yields a maximum slip rate of c. 0.4 mm/a (Figure 10).

#### 4.3.1. Illite Geothermometry

XRD mineralogical evaluations of the fault zone samples show a considerable amount of illite, which is adequate for K-Ar dating (Figure S1 in Supporting Information S1). Illite crystallinity of the footwall lithology samples (UK-15-18 and UK-15-20) ranges from upper diagenetic for the smallest grain size fraction (<0.2 μm) to the lower epizone for the largest grain size fraction (2–6 μm) (KI 0.497 to 0.207°2θ) (Figure 11).

These Illite crystallinity data are in agreement with temperature estimates obtained by RSCM (Figure 9). Samples from lithologies of the hanging wall (UK-15-19 and UK-15-21) show lower illite crystallinity (i.e., higher KI values) and correspond to the middle diagenetic to the lower anchizone (KI 0.601 to 0.399°2θ). As will be discussed in the following, we have reason to believe that our K-Ar age analyses were also affected by a component of inherited illite, which also impacts crystallinity-based geothermometry. However, the predominance of values corresponding to the diagenetic zone in the finest and authigenic-dominated grain size fractions, as well as RSCM temperature estimates, confirm the applicability of K-Ar dating for diagenetic, synkinematic illite in fault gouges.

10.1029/2024TC008660

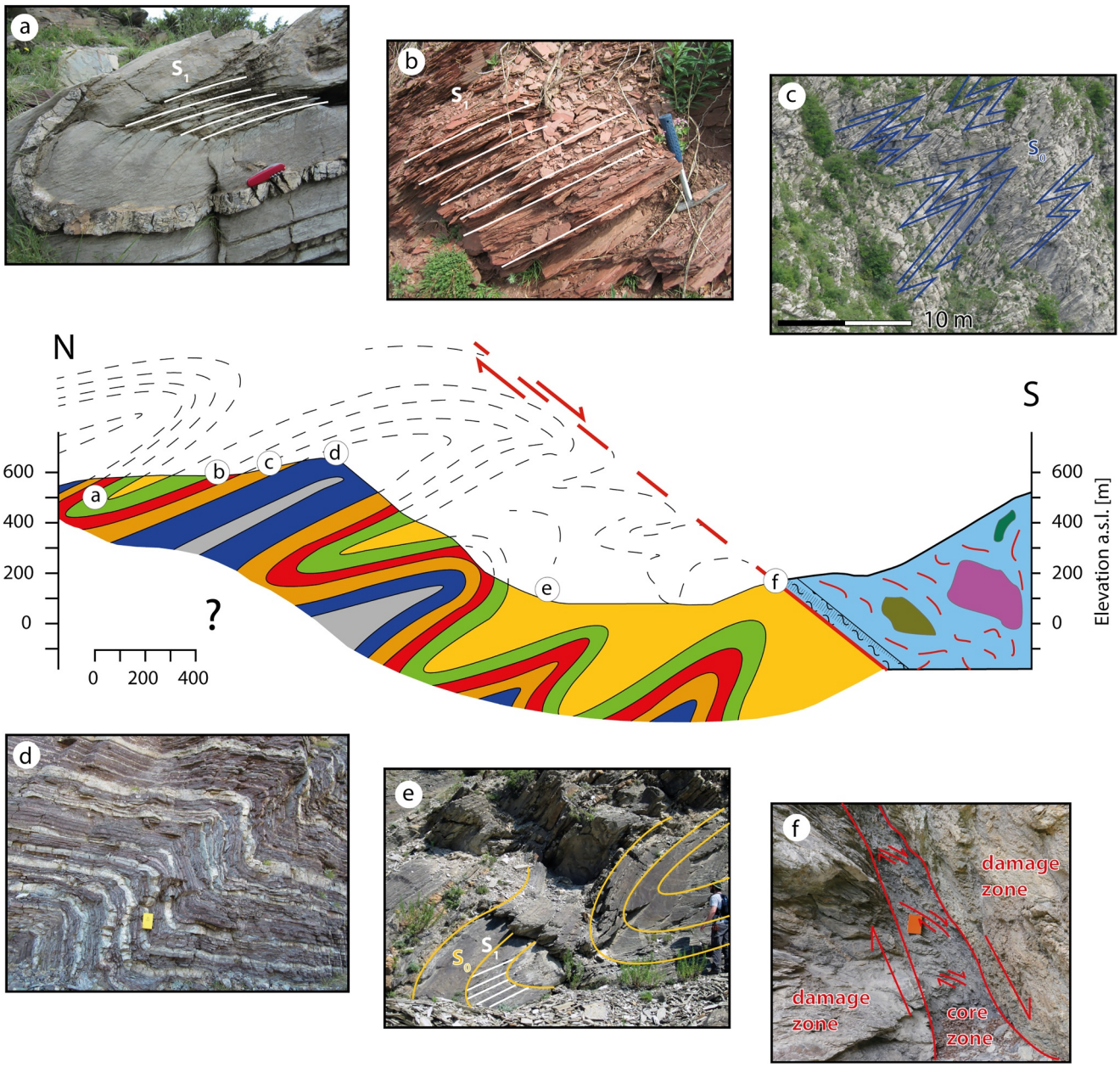


**Figure 7.** N–S oriented cross section through the working area. Top-to-the SSE-directed normal faulting along the Shkoder-Peja Normal Fault (SPNF) truncated large scale south-vergent folds of the footwall. (a) Synclinal hinge of a similar fold showing axial plane cleavage in marly layers and hinge thickening (b) red slates (c) intensely folded calcareous turbidites. (d) Radiolarites (e) tightly folded calcareous slates, marls, silt and claystones. (f) c. 0.5–1 m wide core zone of the SPNF separating intensely folded $Cr_m$-$Pg_1$ calcareous slates, marls, silt- and claystones (N) from ophiolitic tectonic mélange (S). For localization and lithological legend see Figures 2 and 5.

#### 4.3.2. K-Ar Geochronology

The four samples selected for K-Ar dating yield dates ranging between 52.6 Ma (Lutetian) and 105.9 Ma (Albian) for the footwall lithology samples (UK-15-18 and UK-15-20) and between 47.1 (Lutetian) and 69.2 Ma (Maastrichtian) for the hanging wall lithology samples (Table 2 & Figure 12). All data sets except those in sample UK-15-20 show a typical younging trend from coarser to finer grain size fractions, as typical for illite geochronology (Hueck et al., 2022).

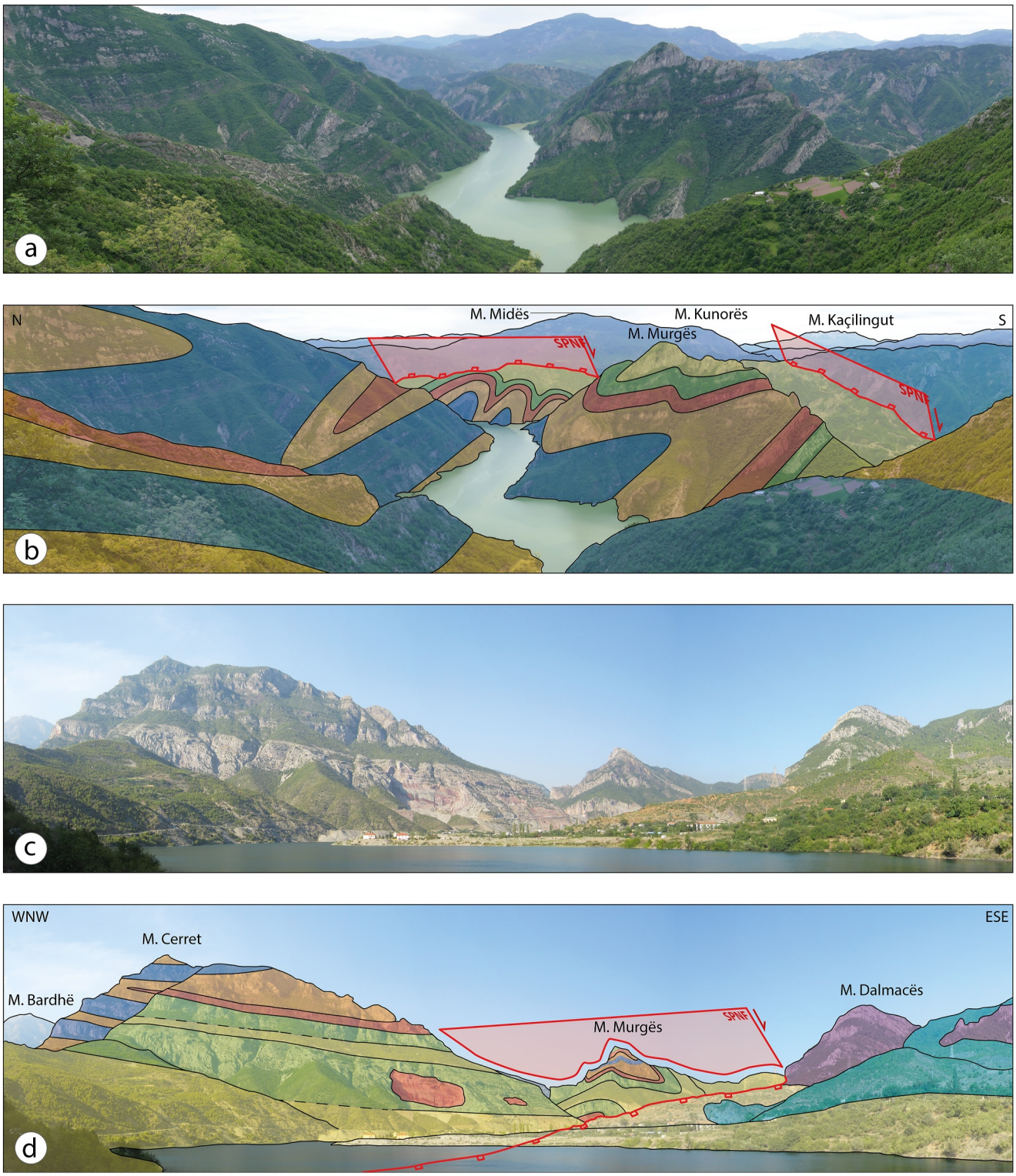


**Figure 8.** (a) Panoramic view from north of the Marsholl village towards the east over the Komani Lake. (b) Geological interpretation of the view along the slightly eastward plunging axes of the folded Krasta-Cukali Unit. (c) Panorama view from the foot of the Kodra Hijes hill toward NNE along the Drin River. (d) Geological interpretation of the southern rim of the Cukali Dome. Folds of the footwall are cut by the Shkoder-Peja Normal Fault, separating it from a smoother landscape in the SSW. Colors in the interpretations are equivalent to those in Figure 5.

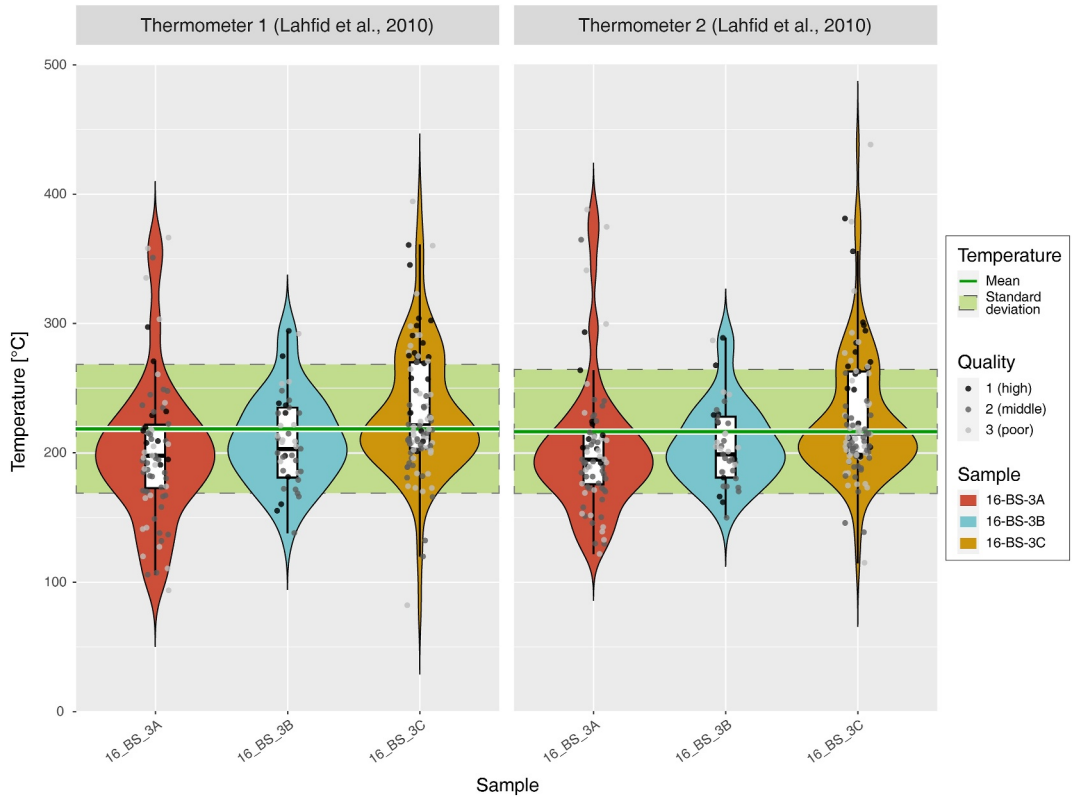


**Figure 9.** Results of Raman spectroscopy of carbonaceous matter (RSCM) measurements of samples 16-BS-3 A–C from different carbon-rich layers of Eocene (?) marls in the footwall of the Shkoder-Peja Normal Fault. Mean temperatures were calculated according to the low-grade thermometer proposed by Lahfid et al. (2010). For localization see Figure 5. Quality ranking is based on the location of the measurement within the carbonaceous material, its coverage as well as its degree of weathering sensu Borrego et al. (2006). Figure created using R statistical software v4.1.2 R Core Team (2021) with the ggplot2 package v3.3.6 (Wickham, 2016).

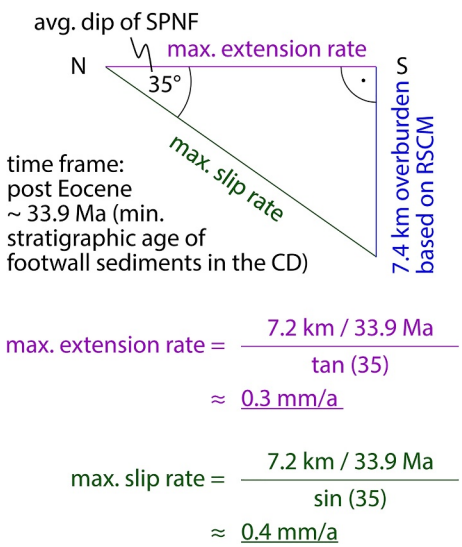


**Figure 10.** Trigonometric calculation of slip rates along the Shkoder-Peja Normal Fault, based on geometric reconstruction of the removed overburden as well as on Raman spectroscopy of carbonaceous matter (RSCM) temperature measurements in the footwall. CD = Cukali Dome.

### 4.3.3. Illite Age Analysis

The analysis of the illite polytypes revealed a considerable share of the $2M_1$ polytype for all samples, which is considered inherited (Figure 12). This means that none of the measured K-Ar dates postdate the inferred minimum depositional age of the youngest lithostratigraphic unit in the footwall of the SPNF (Eocene). This in turn implies that none of our dates directly constrain the age of normal faulting, but, at best, yield mixed detrital (or low-grade metamorphic) and synkinematic ages. By quantifying the relative abundance of different illite polytypes for all fractions (Figure S6 in Supporting Information S1), it is possible to extrapolate end-member ages for the authigenic illite in the sample, a procedure known as illite age analysis (IAA, e.g. Pevear, 1999; van der Pluijm et al., 2001). While this approach may not be applicable in all cases (see Hueck et al., 2022), the clear effect of inherited white mica regarding the inferred dates and the geothermometric results in this study suggest that it is the best strategy for interpreting the available data.

The modeled ages of the authigenic $1M/1M_d$ polytype obtained by IAA are significantly younger (6.2–34.4 Ma) than the mixed ages (47.1–105.9 Ma) and younger than the depositional age of the presumed source rocks (Figure 13).

Sample UK-15-20, on the other hand, has a less-defined trend of uncorrelated dates and grain sizes and therefore did not meet the requirements for IAA.

10.1029/2024TC008660

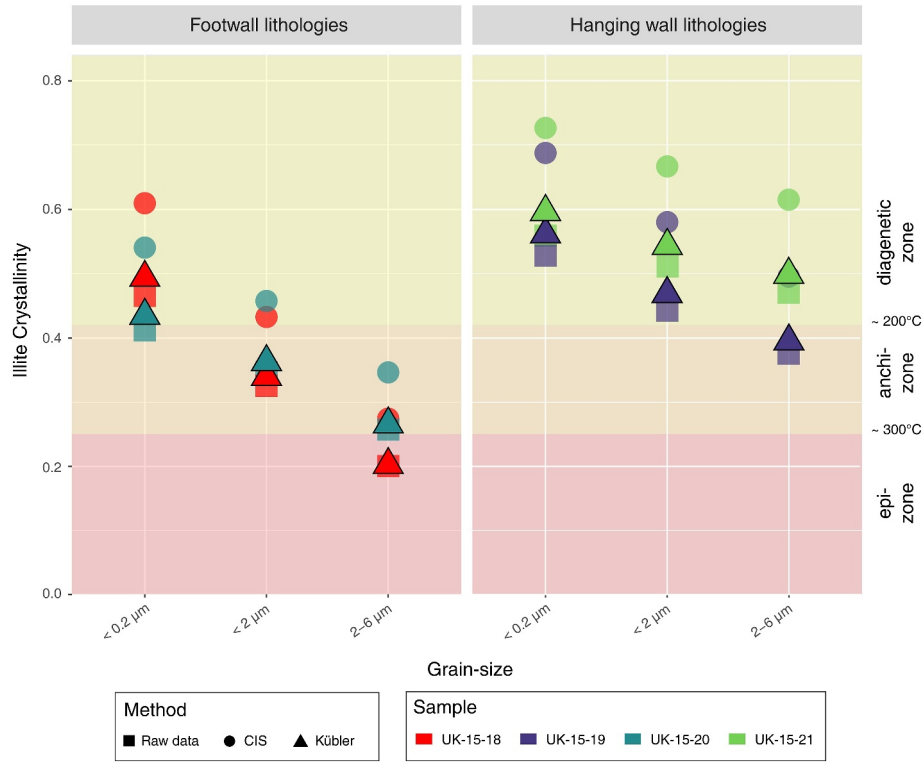


**Figure 11.** Metamorphic grades for all grain size fractions of samples UK-15-18 to UK-15-21 derived from illite geothermometry measured as full width at half maximum (FWHM) of raw data, values calibrated to the Crystallinity Index Standards (CIS) following Warr and Rice (1994) and Warr (2018), and values recalculated from the CIS scale to the Kübler Index (KI) using the equation from Warr and Ferreiro Mählmann (2015). Metamorphic zones vary from upper diagenetic to the lower epizone for the footwall lithologies and from middle diagenetic to lower anchizone for the hanging wall lithologies. All samples show an increasing crystallinity (i.e., lower FWHM values and higher temperatures) with coarsening grain sizes. KI threshold value between diagenesis and anchizone = 0.42; threshold value between anchizone and epizone = 0.25.

Because the ages of the individual dates do not overlap, it also cannot be interpreted as capturing a "pure" inherited or authigenic age. It was therefore excluded from further interpretations.

## 5. Discussion

### 5.1. Fault-Related Fabrics

The identification of distinct brittle structural facies (BSF, sensu Tartaglia et al., 2020) in the field was difficult due to the anisotropic mechanical properties of the layered sedimentary rocks of the footwall and the dominantly scaly fabric (Vannucchi, 2019) of the hanging wall slates and argillites. This manifests itself in distributed strain rather than a localized fault core with sharp BSF boundaries (Carlini et al., 2019). The sedimentary rocks involved in the fault zone deformed via cataclasis and pressure solution creep and therefore produced less distinct contrasts in deformed rock fabrics compared to magmatic and/or metamorphic rocks faulted at the brittle-ductile transition. This resulted in a blurring of cross-cutting relationships that are essential for BSF identification. A posteriori, we would therefore attribute the encountered fault-related fabrics along the SPNF to only three BSFs (Figure 6). These are, from rim to core: (a) The partly still cohesive, comminuted and foliated equivalent of the respective footwall and hanging wall source rocks within the core zone (which could be identified by their different color and carbonate content) forms BSF 1. (b) The c. 1 cm wide direct contact zone of finely ground silty to clayey material between footwall and hanging wall lithologies forms BSF 2. (c) Lastly, the clay-rich, largely incohesive gouge forming an often-diffuse network of cm-scale faults that appeared to traverse the entire core zone, with no discernible systematic cross-cutting relationships forms BSF 3. Only the fault gouges from BSF 3 were sampled for our study (Section 3.1).

10.1029/2024TC008660

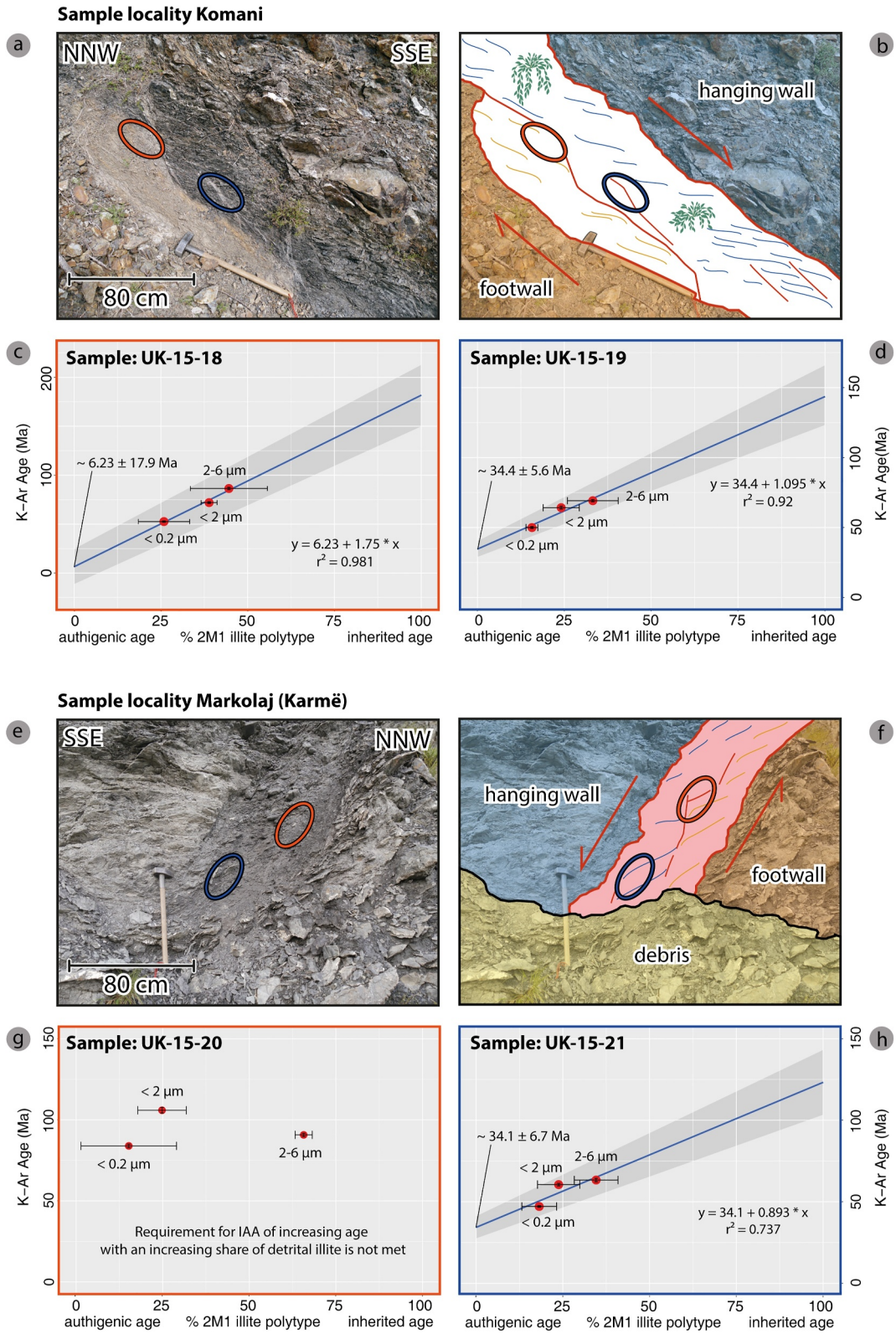


**Figure 12.**

**Table 2**
*Results of K-Ar Dating*

| Sample and grain size fraction | $K_2O$ [Wt. %] | $^{40}Ar$ * [nl/g] STP | $^{40}Ar$ * [%] | Age [Ma] | 2s-Error [Ma] | 2s-Error [%] |
|---|---|---|---|---|---|---|
| Footwall derived lithologies | | | | | | |
| UK 15–18 <0.2 μm | 5.13 | 8.83 | 91.46 | 52.6 | 0.7 | 1.2 |
| UK 15–18 <2 μm | 5 | 11.83 | 92.27 | 72.0 | 0.9 | 1.3 |
| UK 15–18 2-6 μm | 3.88 | 11.06 | 95.92 | 86.4 | 1.2 | 1.4 |
| UK 15–20 <0.2 μm | 3.88 | 10.74 | 83.12 | 83.9 | 1.1 | 1.3 |
| UK 15–20 <2 μm | 4.1 | 14.43 | 91.45 | 105.9 | 1.7 | 1.6 |
| UK 15–20 2-6 μm | 5.21 | 15.63 | 91.14 | 90.7 | 1 | 1.1 |
| Hanging wall derived lithologies | | | | | | |
| UK 15–19 <0.2 μm | 3.33 | 5.43 | 85.3 | 50.0 | 0.7 | 1.4 |
| UK 15–19 <2 μm | 3.55 | 7.47 | 86.19 | 64.2 | 1 | 1.5 |
| UK 15–19 2-6 μm | 3.5 | 7.96 | 88.05 | 69.2 | 0.8 | 1.1 |
| UK 15–21 <0.2 μm | 5.42 | 8.35 | 90.91 | 47.1 | 0.5 | 1.1 |
| UK 15–21 <2 μm | 4.93 | 9.78 | 93.41 | 60.5 | 0.8 | 1.3 |
| UK 15–21 2-6 μm | 5.14 | 10.67 | 95.71 | 63.3 | 1.1 | 1.7 |

### 5.2. Thermal Maturity and Significance of K-Ar Ages for the Timing of the SPNF

Our KI and RSCM analyses indicate that the necessary thermal conditions for the growth of illite, i.e., temperatures above c. 100°C, were reached in all samples. This implies that, in principle, the dated fault gouges should document the authigenic growth of synkinematic illite. Our KI analyses furthermore show that thermal conditions in the footwall were c. 100°C higher than in the hanging wall (Figure 11).

Out of four samples dated, three show a systematic decrease of K-Ar dates with decreasing grain size (UK-15-21, UK-15-19 and UK-15-18), whereas one sample did not show this relationship (UK-15-20). In the case of the samples derived from the hanging wall (UK-15-19 and UK-15-21), all grain size fractions gave K-Ar dates younger than the supposed depositional age range (c. 170–140 Ma) of the subophiolitic tectonic mélange they derived from (Figure 13). In combination with the contrasting thermal conditions of hanging wall and footwall samples (see above), this leads us to interpret the measured ages as detrital and authigenic illite fractions that were mixed in the fault zone (Figure 13).

In the case of footwall sample UK15-18, the measured K-Ar ages partly overlap with the depositional age range (c. 72–34 Ma) of the youngest mappable unit, from which they were sampled. This also suggests a mixed detrital and authigenic origin of the dated illite fractions.

The second footwall sample that did not show a systematic decrease of age and grain size relationship (UK-15-20) can be attributed to either analytical or geological factors. Analytical explanations include potential sample contamination or insufficient separation of grain size fractions. However, this is not supported by any abnormalities in the KI; these samples rather show the expected trend of increasing crystallinity with increasing grain size. Hence, sample contamination or insufficient separation of grain size fractions is unlikely. Geological explanations may involve a heterogeneous origin of the sample material, partial resetting or ripening of the coarser grain-size populations (Zwingmann & Mancktelow, 2004) or the mixing of illite populations formed during

**Figure 12.** Field pictures (a and e), structural interpretation (b and f), and IAA (c, d, g, and h) of the fault gouges sampled for K-Ar dating along the Shkoder-Peja Normal Fault. Color-coded frames of the IAA diagrams correspond to the circles of sample origin within the field pictures and structural interpretations. For localization see Figure 5 and Table 1. The IAA diagrams show the calculation of extrapolated ages from measured mixed dates, according to the share of inherited illite ($2M_1$ polytype). The *y*-axis intercept corresponds to the calculated age of 100% authigenic illite. UK-15-18: footwall lithology fault gouge sampled along the main fault line. UK-15-19: hanging wall lithology fault gouge along a major side branch of the fault. UK-15-20: footwall lithology fault gouge. The requirement for IAA of increasing age with an increasing share of detrital illite is not met in this sample. The estimation of the exclusively authigenic illite is therefore not possible. UK-15-21: hanging wall lithology fault gouge.

10.1029/2024TC008660

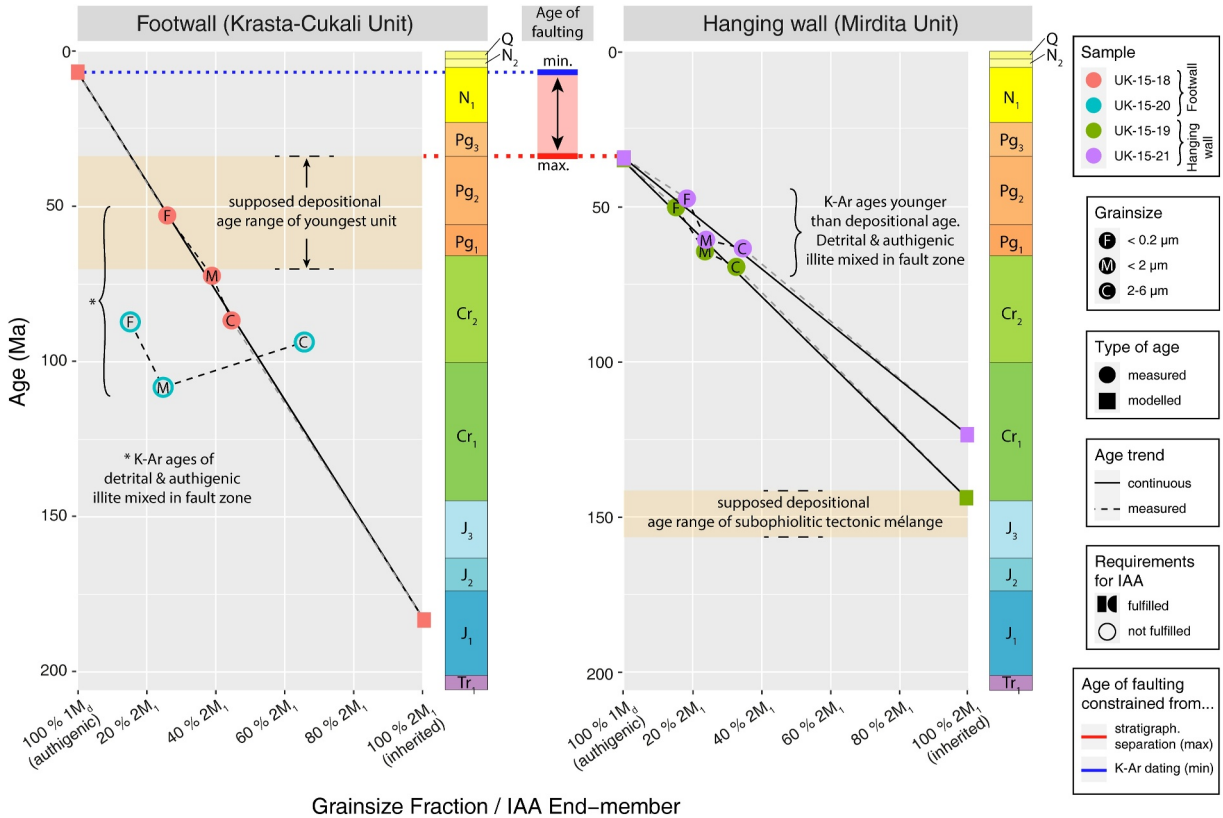


**Figure 13.** Measured illite dates and modeled end-member ages of all dated fault gouges from the Shkoder-Peja Normal Fault in a spatio-temporal context. Requirements for IAA are not met for sample UK-15-20 and should therefore be disregarded. The age trends of the hanging wall samples, on the other hand, show a similar course to each other. The ages of the authigenic illites (0% $2M_1$ polytype) of all valid analyses are below the respective deposition ages.

different faulting events, each with distinct age-grain size characteristics. Any of these causes contradict the fundamental assumptions of a linear age trend and therefore preclude the application of the IAA.

The IAA-modeled end members for the 100% detrital illite age fractions yielded Cretaceous to Jurassic ages for the hanging wall and footwall, respectively. Within the error range of the IAA ages, this is in agreement with the possible age range expected for detrital input in both the Late Jurassic to Early Cretaceous subophiolitic tectonic mélange (hanging wall) as well as the turbiditic marly litharenites to slates of the footwall.

The IAA-modeled end members for the 100% authigenic illite fraction range from c. 34 Ma to 6 Ma in the hanging wall and footwall, respectively. Both these IAA-modeled ages are significantly younger than the depositional age of the stratigraphic units involved, and thus clearly related to fault activity along the SPNF (Bense et al., 2014; Torgersen et al., 2015; Viola et al., 2016).

The considerable error range in the ages of the modeled authigenic illite formation (especially of sample UK-15-18 from the footwall) could be attributed to the variety of possible interpretations of the XRD spectra during polytype analysis and/or in relying only on the minimum required three grain size fractions for IAA analysis. Future studies should perhaps consider incorporating additional fractions to enhance statistical regression accuracy, thereby narrowing the error range. It is also possible that even multiple generations of authigenic illite are present in the samples (Bense et al., 2014; Torgersen et al., 2015; Viola et al., 2016), which could have an impact in the modeled ages that is difficult to estimate. The higher fraction of detrital illite in the footwall (15.2%–65.7%) compared to the hanging wall (15.7%–34.6%) could be an explanation for the larger age spread in the footwall samples. On the other hand, this could also be attributed to the fact that detrital material in the different stratigraphic units has different, mixed ages itself and would therefore cause a different impact on the measured dates. However, further studies support a Late Miocene or even younger fault activity: In their thermochronological study of southern Albania, Rossetti et al. (2024) conclude that deep underplating was triggered at 5–6 Ma in the course of progressing

continental subduction. Even though they primarily associate exhumation of deeper units and extension in the hinterland of southern Albania with the related rollback processes, the lateral discontinuity and, consequently, the disparate pull force exerted by the subducting slab is causative for the rotation of the southern Balkan Peninsula and thus correlated to activity along the SPNF, which serves as a hinge (Handy et al., 2019). Grund et al. (2023) constrain the youngest activity in the eastern section of the SNPF (along what they refer to as "Dukagjini Fault") to the latest Miocene, claiming that Miocene syn-rift sediments are unconformably overlain by Plio-Pleistocene post-rift sediments in parts of the western Kosovo Basin. However, we regard their analysis as flawed since they misinterpreted the continuation of the trace of the SPNF into Kosovo by "inventing" a buried fault that is supposedly independent from the SPNF. Gürbüz et al. (2024), based on extensive geomorphic and structural analyses in western Kosovo, clearly demonstrated ongoing neotectonic activity along the N–S striking fault segment of the SPNF south of Peja (named Peja Fault) and its continuation along the WSW-ENE striking segment east of Peja (named Istog Fault), both rimming the adjacent Dukagjini Basin (see Figure 2). Recent deformation along the Peja Fault segment was also noted by GNSS studies and tectonic geomorphological observations of D'Agostino et al. (2022).

The above-mentioned evidence for ongoing deformation is not inconsistent with our results, as the following three factors must be considered: (a) More recent fault activity at temperatures lower than those required by the methodology used in this study is explicitly not excluded, and is simply outside the temperature range for authigenic illite formation required for radiometric dating. In order to gain further insight into the dynamics of fault activity at lower temperatures, future studies should consider electron spin resonance and optically stimulated luminescence dating (e.g., Prince et al., 2024) as supplementary methods to the present study. (b) A less conservative approach, which does not exclude possible overlap of other minerals within the range of peaks diagnostic for the illite polytype quantification (e.g., albite), would result in even younger IAA modeled authigenic illite ages, albeit at the expense of an even higher error range. (c) Our structural characterization and sampling strategy may have missed out younger BSF (sensu Tartaglia et al., 2020), as already two different authigenic IAA-ages had been detected within the designated BSF 3. Probably, the strain was not localized enough to create a single, well-defined fault surface, but rather anastomosing branches within an up to 20 m wide fault zone.

Nevertheless, we conclude that the determination of two distinct authigenic illite ages by IAA and therefore fault activity aligns well with the tectonic context. This conclusion allows the interpretation either of a continuous fault activity that began no later than Early Oligocene and continued at least into Late Miocene, or alternatively, of an episodic reactivation with at least two separate periods of activity during this time span (Oligocene and Miocene).

In view of a number of recent GNSS and geomorphic studies, we consider it likely that parts of the SPNF are still actively accommodating extensional deformation.

## 6. Conclusions

1. Detailed mapping and geometric considerations give further proof of a post-Eocene brittle normal faulting character of the SPNF. Outcrop-scale kinematic indicators are consistent with map-scale considerations and indicate top-to-the SSE normal faulting.
2. The average observed fault dip of 35° and an estimated overburden of c. 7 km indicated by RSCM-derived temperatures implies a minimum of c. 13 km post-Eocene fault-parallel displacement. A conservative estimate of the fault slip rate therefore amounts to c. 0.4 mm/a.
3. Two age clusters for the authigenic $1M/1M_d$ polytype illite were modeled by IAA for the sampled fault gouges: One for the Early Oligocene and one for the Late Miocene. Both could possibly be linked to separate geological events: the onset of normal faulting in the study area based on cross-cutting relationships and a renewed tectonic phase of exhumation in the southern Albanian Hellenides triggered by the onset of rollback of the Adriatic slab, respectively.
4. In consideration of the two age clusters and the anastomosing nature of the fault, with some strands not sampled, both a continuous or a (at least) biphasic activity of the SPNF since the Early Oligocene are possible. A later fault activity at temperatures below the formation temperature of illite is conceivable.
5. This study demonstrates that, despite the limited data sets and the partially large ranges of error, meaningful insights can be obtained by systematically integrating a variety of data sources and methods.

## Conflict of Interest

The authors declare no conflicts of interest relevant to this study..

## Data Availability Statement

The XRD and Raman data used for quantitative and qualitative mineralogical investigations as well as peak metamorphic ranges and illite age analysis in the study are available at Zenodo via https://doi.org/10.5281/zenodo.15437195. A high resolution, editable version of the geological map of the study area (Figure 5) including dip angles that have been hidden in the version contained in this paper for reasons of better readability via https://doi.org/10.5281/zenodo.15511931. All under Creative Commons Attribution 4.0 International licenses.

**Acknowledgments**

We thank Mark Handy, Jörg Giese and Marc Grund (FU Berlin) for stimulating scientific discussions. Marko Vrabec (University of Ljubljana) for drone imagery as well as Bardhyl Muceku, Gezim Tola (Polytechnical University Tirana) and numerous MSc students from FSU Jena, MLU Halle-Wittenberg and RWTH Aachen who helped during field work. We are grateful for the guidance during XRD analysis given by Maria Wierzbicka-Wieczorek and Ralph Bolanz (FSU Jena) as well as Georg Löwe and Philipp Balling (FSU Jena) for improvements on an earlier version of the manuscript. Open-source software Stereonet and Innstereo were used for creating stereoplots and Fityk for evaluation of Raman spectra as well as R for statistical analysis and illustration. We furthermore thank Giulio Viola and an anonymous reviewer for their diligence and constructive criticism that helped to improve our study. Lastly, we thank Djordje Grujic for editorial handling paired with additional helpful comments. Funding of the project ALMOND ("Albania Montenegro Neotectonic Deformation," project number 269913092) by Deutsche Forschungsgemeinschaft (DFG) granted to Kamil Ustaszewski and Klaus Reicherter is gratefully acknowledged. Open Access funding enabled and organized by Projekt DEAL.

## References

Aubouin, J., Blanchet, R., Cadet, J.-P., Celet, P., Charvet, J., Chorowicz, J., et al. (1970). Essai sur la géologie des Dinarides. *Bulletin de la Societe Geologique de France*, *7*, 1060–1095.

Aubouin, J., & Dercourt, J. (1975). Les transversales dinariques, derivent-elles de paleofailles transformantes? *Compte-Rendu Académie des Sciences Série D*, *281*, 347–350.

Aliaj, S., Baldassarre, G., & Shkupi, D. (2001). Quaternary subsidence zones in Albania: Some case studies. *Bulletin of Engineering Geology and the Environment*, *59*(4), 313–318. https://doi.org/10.1007/s100640000063

Balling, P., Grützner, C., Tomljenović, B., Spakman, W., & Ustaszewski, K. (2021). Post-collisional mantle delamination in the Dinarides implied from staircases of Oligo-Miocene uplifted marine terraces. *Scientific Reports*, *11*(1), 2685. https://doi.org/10.1038/s41598-021-81561-5

Balling, P., Tomljenović, B., Herak, M., & Ustaszewski, K. (2023). Impact of mechanical stratigraphy on deformation style and distribution of seismicity in the central External Dinarides: A 2D forward kinematic modelling study. *Swiss Journal of Geosciences*, *116*(1), 7. https://doi.org/10.1186/s00015-023-00437-0

Balling, P., Tomljenović, B., Schmid, S. M., & Ustaszewski, K. (2021). Contrasting along-strike deformation styles in the central external Dinarides assessed by balanced cross-sections: Implications for the tectonic evolution of its Paleogene flexural foreland basin system. *Global and Planetary Change*, *205*, 103587. https://doi.org/10.1016/j.gloplacha.2021.103587

Bense, F. A., Wemmer, K., Löbens, S., & Siegesmund, S. (2014). Fault gouge analyses: K–Ar illite dating, clay mineralogy and tectonic significance—A study from the Sierras Pampeanas, Argentina. *International Journal of Earth Sciences*, *103*(1), 189–218. https://doi.org/10.1007/s00531-013-0956-7

Bernoulli, D., & Laubscher, H. (1972). The palinspastic problem of the Hellenides. *Eclogae Geologicae Helvetiae*, *65*, 107–118.

Bijwaard, H., & Spakman, W. (2000). Non-linear global P -wave tomography by iterated linearized inversion. *Geophysical Journal International*, *141*(1), 71–82. https://doi.org/10.1046/j.1365-246X.2000.00053.x

Borrego, A. G., Araujo, C. V., Balke, A., Cardott, B., Cook, A. C., David, P., et al. (2006). Influence of particle and surface quality on the vitrinite reflectance of dispersed organic matter: Comparative exercise using data from the qualifying system for reflectance analysis working group of ICCP. *International Journal of Coal Geology*, *68*(3–4), 151–170. https://doi.org/10.1016/j.coal.2006.02.002

Burchfiel, B. C., King, R. W., Nakov, R., Tzankov, T., Dumurdzanov, N., movski, T. S., et al. (2008). Patterns of Cenozoic extensional tectonism in the south Balkan extensional system, in: Earthquake monitoring and seismic hazard mitigation in Balkan countries: Proceedings of the NATO advanced research workshop on earthquake monitoring and seismic hazard mitigation. In E. S. Husebye (Ed.), *Balkan countries, Borovetz, Bulgaria, 11 - 18 September 2005* (pp. 3–18). Springer. https://doi.org/10.1007/978-1-4020-6815-7_1

Carlini, M., Viola, G., Mattila, J., & Castellucci, L. (2019). The role of mechanical stratigraphy on the refraction of strike-slip faults. *Solid Earth*, *10*(1), 343–356. https://doi.org/10.5194/se-10-343-2019

Cionoiu, S., Zertani, S., Handy, M. R., Onuzi, K., & Ustaszewski, K. (2014). Changes in style of deformation along the Dinaric-Hellenic chain in northern Albania and southern Montenegro (p. 1).

D'Agostino, N., Avallone, A., Cheloni, D., D'Anastasio, E., Mantenuto, S., & Selvaggi, G. (2008). Active tectonics of the Adriatic region from GPS and earthquake slip vectors. *Journal of Geophysical Research*, *113*(B12), B09401. https://doi.org/10.1029/2008JB005860

D'Agostino, N., Copley, A., Jackson, J., Koçi, R., Hajrullai, A., Duni, L., & Kuka, N. (2022). Active tectonics and fault evolution in the Western Balkans. *Geophysical Journal International*, *231*(3), 2102–2126. https://doi.org/10.1093/gji/ggac316

D'Agostino, N., Métois, M., Koci, R., Duni, L., Kuka, N., Ganas, A., et al. (2020). Active crustal deformation and rotations in the southwestern Balkans from continuous GPS measurements. *Earth and Planetary Science Letters*, *539*, 116246. https://doi.org/10.1016/j.epsl.2020.116246

Doebelin, N., & Kleeberg, R. (2015). Profex: A graphical user interface for the Rietveld refinement program BGMN. *Journal of Applied Crystallography*, *48*(5), 1573–1580. https://doi.org/10.1107/S1600576715014685

Dumurdzanov, N., Serafimovski, T., & Burchfiel, B. C. (2005). Cenozoic tectonics of Macedonia and its relation to the South Balkan extensional regime. *Geosphere*, *1*, 1–22. https://doi.org/10.1130/GES00006.1

Festa, A., Pini, G. A., Ogata, K., & Dilek, Y. (2019). Diagnostic features and field-criteria in recognition of tectonic, sedimentary and diapiric mélanges in orogenic belts and exhumed subduction-accretion complexes. *Gondwana Research*, *74*, 7–30. https://doi.org/10.1016/j.gr.2019.01.003

Fettes, D. J., & Desmons, J. (2007). *Metamorphic rocks: A classification and glossary of terms recommendations of the International Union of Geological Sciences Subcommission on the Systematics of Metamorphic Rocks* (p. 244). Cambridge University Press.

Fossen, H., & Cavalcante, G. C. G. (2017). Shear zones – A review. *Earth-Science Reviews*, *171*, 434–455. https://doi.org/10.1016/j.earscirev.2017.05.002

Friedrich, D. (1991). *Eine neue Methode zur Bestimmung der Illit Kristallinität mit Hilfe digitaler Meßwerterfassung: Unpublished*. PhD Thesis (p. 63). University of Göttingen.

Fuhrmann, U., Lippolt, H. J., & Hess, J. C. (1987). Examination of some proposed K-Ar standards: Analyses and conventional K-Ar data. *Chemical Geology: Isotope Geoscience section*, *66*(1–2), 41–51. https://doi.org/10.1016/0168-9622(87)90027-3

Gawlick, H.-J., & Missoni, S. (2019). Middle-Late Jurassic sedimentary mélange formation related to ophiolite obduction in the Alpine-Carpathian-Dinaridic Mountain Range. *Gondwana Research*, *74*, 144–172. https://doi.org/10.1016/j.gr.2019.03.003

Gerzina, N., & Djeric, N. (2016). Chert blocks in the ophiolitic mélange of Zlatibor Mt. (SW Serbia): Age and geodynamic implications. *Geol An Balk Poluos*(77), 13–21. https://doi.org/10.2298/GABP1677013G

Grathoff, G. H., & Moore, D. M. (1996). Illite polytype quantification using WILDFIRE© calculated X-ray diffraction patterns. *Clays and Clay Minerals*, *44*(6), 835–842. https://doi.org/10.1346/CCMN.1996.0440615

Grathoff, G. H., Moore, D. M., Hay, R. L., & Wemmer, K. (2001). Origin of illite in the lower Paleozoic of the Illinois basin: Evidence for brine migrations. *GSA Bulletin*, *113*(8), 1092–1104. https://doi.org/10.1130/0016-7606(2001)113%3C1092:OOIITL%3E2.0.CO;2

Grund, M. U. (2023). *The Shkoder Peja Normal Fault system at the Dinaric-Hellenic Junction: A structural and thermochronological study*. Freie Universität Berlin.

Grund, M. U., Handy, M. R., Giese, J., Gemignani, L., Pleuger, J., & Onuzi, K. (2023). Faulting, basin formation and orogenic arcuation at the Dinaric–Hellenic junction (northern Albania and Kosovo). *International Journal of Earth Sciences*, *112*(6), 1613–1634. https://doi.org/10.1007/s00531-023-02318-1

Gürbüz, A., Shala, A., Mustafa, S., & Erten, A. (2024). Active tectonics of western Kosova: Insights from geomorphic and structural analyses. *Bull.Min.Res.Exp.*, 153–173. https://doi.org/10.19111/bulletinofmre.1186708

Handy, M. R., Giese, J., Schmid, S. M., Pleuger, J., Spakman, W., Onuzi, K., & Ustaszewski, K. (2019). Coupled crust-mantle response to slab tearing, bending, and rollback along the Dinaride-Hellenide orogen. *Tectonics*, *281*(8), 11–2828. https://doi.org/10.1029/2019TC005524

Heitzmann, P. (1987). Evidence of late oligocene/early miocene backthrusting in the central alpine "root zone". *Geodinamica Acta*, *1*(3), 183–192. https://doi.org/10.1080/09853111.1987.11105137

Hueck, M., Wemmer, K., Basei, M. A., Philipp, R. P., Oriolo, S., Heidelbach, F., et al. (2020). Dating recurrent shear zone activity and the transition from ductile to brittle deformation: White mica geochronology applied to the Neoproterozoic Dom Feliciano Belt in South Brazil. *Journal of Structural Geology*, *141*, 104199. https://doi.org/10.1016/j.jsg.2020.104199

Hueck, M., Wemmer, K., Ksienzyk, A. K., Kuehn, R., & Vogel, N. (2022). Potential, premises, and pitfalls of interpreting illite argon dates - A case study from the German Variscides. *Earth-Science Reviews*, *232*, 104133. https://doi.org/10.1016/j.earscirev.2022.104133

Jolivet, L., Faccenna, C., & Piromallo, C. (2009). From mantle to crust: Stretching the Mediterranean. *Earth and Planetary Science Letters*, *285*(1–2), 198–209. https://doi.org/10.1016/j.epsl.2009.06.017

Jouanne, F., Mugnier, J. L., Koci, R., Bushati, S., Matev, K., Kuka, N., et al. (2012). GPS constraints on current tectonics of Albania. *Tectonophysics*, *554–557*, 50–62. https://doi.org/10.1016/j.tecto.2012.06.008

Kissel, C., Speranza, F., & Milicevic, V. (1995). Paleomagnetism of external southern and central Dinarides and northern Albanides: Implications for the Cenozoic activity of the Scutari-Pec Transverse Zone. *Journal of Geophysical Research*, *100*(B8), 14999–15007. https://doi.org/10.1029/95JB01243

Koulakov, I., Kaban, M. K., Tesauro, M., & Cloetingh, S. (2009). P - And S -velocity anomalies in the upper mantle beneath Europe from tomographic inversion of ISC data. *Geophysical Journal International*, *179*(1), 345–366. https://doi.org/10.1111/j.1365-246X.2009.04279.x

Kralik, M., Klima, K., & Riedmüller, G. (1987). Dating fault gouges. *Nature*, *327*(6120), 315–317. https://doi.org/10.1038/327315a0

Ksienzyk, A. K., Wemmer, K., Jacobs, J., Fossen, H., Schomberg, A. C., Süssenberger, A., et al. (2016). Post-Caledonian brittle deformation in the Bergen area, West Norway: Results from K–Ar illite fault gouge dating. NJG. *Norwegian Journal of Geology*. https://doi.org/10.17850/njg96-3-06

Kübler, B. (1967). La cristallinité de l'illite et les zones tout à fait supérieures du. *Tectonique, Colloque de Neuchâtel*.

Lahfid, A., Beyssac, O., Deville, E., Negro, F., Chopin, C., & Goffé, B. (2010). Evolution of the Raman spectrum of carbonaceous material in low-grade metasediments of the Glarus Alps (Switzerland). *Terra Nova*, *22*(5), 354–360. https://doi.org/10.1111/j.1365-3121.2010.00956.x

Leeuw, A. d., Mandic, O., Krijgsman, W., Kuiper, K., & Hrvatović, H. (2012). Paleomagnetic and geochronologic constraints on the geodynamic evolution of the Central Dinarides. *Tectonophysics*, *530–531*, 286–298. https://doi.org/10.1016/j.tecto.2012.01.004

Löbens, S., Bense, F. A., Wemmer, K., Dunkl, I., Costa, C. H., Layer, P., & Siegesmund, S. (2011). Exhumation and uplift of the Sierras Pampeanas: Preliminary implications from K–Ar fault gouge dating and low-T thermochronology in the Sierra de Comechingones (Argentina). *International Journal of Earth Sciences*, *100*(2–3), 671–694. https://doi.org/10.1007/s00531-010-0608-0

Lünsdorf, N. K., & Lünsdorf, J. O. (2016). Evaluating Raman spectra of carbonaceous matter by automated, iterative curve-fitting. *International Journal of Coal Geology*, *160–161*, 51–62. https://doi.org/10.1016/j.coal.2016.04.008

Lyons, J. B., & Snellenburg, J. (1971). Dating faults. *GSA Bulletin*, *82*(6), 1749. https://doi.org/10.1130/0016-7606(1971)82[1749:DF]2.0.CO;2

Márton, E., Pavelić, D., Vranjković, A., & Ćosović, V. (2016). Reappraisal of the palaeomagnetism of the Miocene intramontane Pag and Drniš–Sinj basins, External Dinarides (Croatia). *Tectonophysics*, *676*, 125–134. https://doi.org/10.1016/j.tecto.2016.03.033

Meço, S., & Aliaj, S. (2000). *Geology of Albania: With 1 table in the text, Beiträge zur regionalen Geologie der Erde* (Vol. 28, p. 246). Borntraeger.

Métois, M., D'Agostino, N., Avallone, A., Chamot-Rooke, N., Rabaute, A., Duni, L., et al. (2015). Insights on continental collisional processes from GPS data: Dynamics of the peri-Adriatic belts. *Journal of Geophysical Research: Solid Earth*, *120*(12), 8701–8719. https://doi.org/10.1002/2015JB012023

Moore, D. M., & Reynolds, R. C. (1997). *X-ray diffraction and identification and analysis of clay minerals* (2nd ed.). Oxford University Press.

Pamić, J. (1993). Eoalpine to Neoalpine magmatic and metamorphic processes in the northwestern Vardar Zone, the easternmost Periadriatic Zone and the southwestern Pannonian Basin. *Tectonophysics*, *226*(1–4), 503–518. https://doi.org/10.1016/0040-1951(93)90135-7

Pamić, J. (2002). The Sava-Vardar Zone of the Dinarides and Hellenides versus the Vardar Ocean. *Eclogae Geologicae Helvetiae*, *95*, 99–113.

Papanikolaou, D. (2013). Tectonostratigraphic models of the Alpine terranes and subduction history of the Hellenides. *Tectonophysics*, *595–596*, 1–24. https://doi.org/10.1016/j.tecto.2012.08.008

Pevear, D. R. (1992). Illite age analysis, a new tool for basin thermal history analysis. In *International symposium on water-rock interaction* (pp. 1251–1254).

Pevear, D. R. (1999). Illite and hydrocarbon exploration. *Proceedings of the National Academy of Sciences of the United States of America*, *96*(7), 3440–3446. https://doi.org/10.1073/pnas.96.7.3440

Pleuger, J., Mancktelow, N., Zwingmann, H., & Manser, M. (2012). K–Ar dating of synkinematic clay gouges from Neoalpine faults of the Central, Western and Eastern Alps. *Tectonophysics*, *550–553*, 1–16. https://doi.org/10.1016/j.tecto.2012.05.001

Prince, E., Tsukamoto, S., Grützner, C., Vrabec, M., & Ustaszewski, K. (2024). Not too old to rock: ESR and OSL dating reveal Quaternary activity of the Periadriatic Fault in the Alps. *Earth Planets and Space*, *76*(1), 85. https://doi.org/10.1186/s40623-024-02015-6

Ramsay, J. G. (1967). Folding and fracturing of rocks. In *International series in the earth and planetary sciences* (p. 568). Blackburn Press.

Randjelovic, N., Matenco, L., Krstekanić, N., Maleš, M., Stojadinović, U., Toljić, M., et al. (2025). Crustal response to slab tearing and detachment: Inferences from the kinematics of the Dinarides-Hellenides transition. *Global and Planetary Change*, *252*, 104837. https://doi.org/10.1016/j.gloplacha.2025.104837

R Core Team. (2021). *R: A language and environment for statistical computing*. R Foundation for Statistical Computing. Retrieved from https://www.R-project.org/

Robertson, A., & Shallo, M. (2000). Mesozoic–Tertiary tectonic evolution of Albania in its regional Eastern Mediterranean context. *Tectonophysics*, *316*(3–4), 197–254. https://doi.org/10.1016/S0040-1951(99)00262-0

Rossetti, F., Fellin, M. G., Ballato, P., Faccenna, C., Balestrieri, M. L., Muceku, B., et al. (2024). Building the albanides by deep underplating. *Tectonics*, *43*(11). https://doi.org/10.1029/2024TC008506

Sadezky, A., Muckenhuber, H., Grothe, H., Niessner, R., & Pöschl, U. (2005). Raman microspectroscopy of soot and related carbonaceous materials: Spectral analysis and structural information. *Carbon*, *43*(8), 1731–1742. https://doi.org/10.1016/j.carbon.2005.02.018

Schefer, S., Egli, D., Missoni, S., Bernoulli, D., Fügenschuh, B., Gawlick, H.-J., et al. (2010). Triassic metasediments in the internal Dinarides (Kopaonik area, southern Serbia): Stratigraphy, paleogeographic and tectonic significance. *Geologica Carpathica*, *61*(2), 89–109. https://doi.org/10.2478/v10096-010-0003-6

Schmid, S. M., Bernoulli, D., Fügenschuh, B., Matenco, L., Schefer, S., Schuster, R., et al. (2008). The Alpine-Carpathian-Dinaridic orogenic system: Correlation and evolution of tectonic units. *Swiss Journal of Geosciences*, *101*(1), 139–183. https://doi.org/10.1007/s00015-008-1247-3

Schmid, S. M., Fügenschuh, B., Kounov, A., Matenco, L., Nievergelt, P., Oberhänsli, R., et al. (2020). Tectonic units of the Alpine collision zone between Eastern Alps and western Turkey. *Gondwana Research*, *78*, 308–374. https://doi.org/10.1016/j.gr.2019.07.005

Schmitz, B. J., & Ustaszewski, K. (2025a). Geological Map Komani, Northern Albania related to the article "Kinematics and age of the orogen-perpendicular Shkoder-Peja Normal Fault in North Albania constrained by fault-slip data, Raman spectroscopy and K-Ar fault-gouge dating" published in Tectonics [Figure]. *Zenodo*. https://doi.org/10.5281/zenodo.15511932

Schmitz, B. J., & Ustaszewski, K. (2025b). Data sets related to the article "Kinematics and age of the orogen-perpendicular Shkoder-Peja Normal Fault in North Albania constrained by fault-slip data, Raman spectroscopy and K-Ar fault-gouge dating" published in Tectonics [Dataset]. *Zenodo*. https://doi.org/10.5281/zenodo.15437196

Schumacher, E. (1975). Herstellung von> 99, 9997% 38Argon für die 40K-40Ar-Geochronologie. *Kurze Mitteilungen*, *29*(10), 441–442. https://doi.org/10.2533/chimia.1975.441

Serretti, P., & Morelli, A. (2011). Seismic rays and traveltime tomography of strongly heterogeneous mantle structure: Application to the Central Mediterranean. *Geophysical Journal International*, *187*(3), 1708–1724. https://doi.org/10.1111/j.1365-246X.2011.05242.x

Sibson, R. H. (1977). Fault rocks and fault mechanisms. *JGS*, *133*(3), 191–213. https://doi.org/10.1144/gsjgs.133.3.0191

Sibson, R. H. (1986). Earthquakes and rock deformation in crustal fault zones. *Annual Review of Earth and Planetary Sciences*, *14*(1), 149–175. https://doi.org/10.1146/annurev.ea.14.050186.001053

Speranza, F., Islami, I., Kissel, C., & Hyseni, A. (1995). Paleomagnetic evidence for Cenozoic clockwise rotation of the external Albanides. *Earth and Planetary Science Letters*, *129*(1–4), 121–134. https://doi.org/10.1016/0012-821X(94)00231-M

Steiger, R. H., & Jäger, E. (1977). Subcommission on geochronology: Convention on the use of decay constants in geo- and cosmochronology. *Earth and Planetary Science Letters*, *36*(3), 359–362. https://doi.org/10.1016/0012-821X(77)90060-7

Sudar, M., & Kovács, S. (2006). Metamorphosed and ductilely deformed conodonts from Triassic limestones situated beneath ophiolite complexes: Kopaonik Mountain (Serbia) and Bukk Mountains (NE Hungary)-a preliminary comparison. *Geologica Carpathica*, *57*, 157–176.

Tari, V., & Pamić, J. (1998). Geodynamic evolution of the northern Dinarides and the southern part of the Pannonian Basin. *Tectonophysics*, *297*(1–4), 269–281. https://doi.org/10.1016/S0040-1951(98)00172-3

Tartaglia, G., Viola, G., van der Lelij, R., Scheiber, T., Ceccato, A., & Schönenberger, J. (2020). "Brittle structural facies" analysis: A diagnostic method to unravel and date multiple slip events of long-lived faults. *Earth and Planetary Science Letters*, *545*, 116420. https://doi.org/10.1016/j.epsl.2020.116420

Torgersen, E., Viola, G., Zwingmann, H., & Henderson, I. H. C. (2015). Inclined K–Ar illite age spectra in brittle fault gouges: Effects of fault reactivation and wall-rock contamination. *Terra Nova*, *27*(2), 106–113. https://doi.org/10.1111/ter.12136

Tsukamoto, S., Tagami, T., & Zwingmann, H. (2020). Direct dating of fault movement. In *Understanding faults: Detecting, dating, and modeling* (pp. 257–282). Elsevier. https://doi.org/10.1016/B978-0-12-815985-9.00007-2

Ustaszewski, K., Schmid, S. M., Lugović, B., Schuster, R., Schaltegger, U., Bernoulli, D., et al. (2009). Late Cretaceous intra-oceanic magmatism in the internal Dinarides (northern Bosnia and Herzegovina): Implications for the collision of the Adriatic and European plates. *Lithos*, *108*(1–4), 106–125. https://doi.org/10.1016/j.lithos.2008.09.010

van der Pluijm, B. A., Hall, C. M., Vrolijk, P. J., Pevear, D. R., & Covey, M. C. (2001). The dating of shallow faults in the Earth's crust. *Nature*, *412*(6843), 172–175. https://doi.org/10.1038/35084053

van Hinsbergen, D., Langereis, C. G., & Meulenkamp, J. E. (2005). Revision of the timing, magnitude and distribution of Neogene rotations in the western Aegean region. *Tectonophysics*, *396*(1–2), 1–34. https://doi.org/10.1016/j.tecto.2004.10.001

Vannucchi, P. (2019). Scaly fabric and slip within fault zones. *Geosphere*, *15*(2), 342–356. https://doi.org/10.1130/GES01651.1

Velde, B. (1965). Experimental determination of muscovite polymorph stabilities. *American Mineralogist*, *50*, 436–449.

Viola, G., Scheiber, T., Fredin, O., Zwingmann, H., Margreth, A., & Knies, J. (2016). Deconvoluting complex structural histories archived in brittle fault zones. *Nature Communications*, *7*(1), 13448. https://doi.org/10.1038/ncomms13448

Vishnevskaya, V. S., Djeric, N., & Zakariadze, G. S. (2009). New data on Mesozoic Radiolaria of Serbia and Bosnia, and implications for the age and evolution of oceanic volcanic rocks in the Central and Northern Balkans. *Lithos*, *108*(1–4), 72–105. https://doi.org/10.1016/j.lithos.2008.10.015

Vrolijk, P., Pevear, D., Covey, M., & LaRiviere, A. (2018). Fault gouge dating: History and evolution. *Clay Minerals*, *53*(3), 305–324. https://doi.org/10.1180/clm.2018.22

Vrolijk, P., & van der Pluijm, B. A. (1999). Clay gouge. *Journal of Structural Geology*, *21*(8–9), 1039–1048. https://doi.org/10.1016/S0191-8141(99)00103-0

Warr, L. N. (2018). A new collection of clay mineral 'Crystallinity' Index Standards and revised guidelines for the calibration of Kübler and Árkai indices. *Clay Minerals*, *53*(3), 339–350. https://doi.org/10.1180/clm.2018.42

Warr, L. N., & Ferreiro Mählmann, R. (2015). Recommendations for Kübler Index standardization. *Clays and Clay Minerals*, *50*, 283–286. https://doi.org/10.1180/claymin.2015.050.3.02

Warr, L. N., & Rice, A. H. N. (1994). Interlaboratory standardization and calibration of day mineral crystallinity and crystallite size data. *Journal of Metamorphic Geology*, *12*(2), 141–152. https://doi.org/10.1111/j.1525-1314.1994.tb00010.x

Wemmer, K. (1991). K/Ar-Altersdatierungsmöglichkeiten für retrograde Deformationsprozesse K/Ar-Altersdatierungsmöglichkeiten für retrograde Deformations-prozesse im spröden und duktilen Bereich — Beispiele aus der KTB-Vorbohrung (Oberpfalz) und dem Bereich der Insubrischen Linie (N-Italien). (Oberpfalz) und dem Bereich der Insubrischen Linie (N-Italien). *Göttinger Arbeiten zur Geologie und Paläontologie*, *51*, 1–61.

Wickham, H. (2016). *ggplot2: Elegant graphics for data analysis* (2nd ed., Use R, p. 260). Springer international publishing.

Zwingmann, H., & Mancktelow, N. (2004). Timing of Alpine fault gouges. *Earth and Planetary Science Letters*, *223*(3–4), 415–425. https://doi.org/10.1016/j.epsl.2004.04.041

Zwingmann, H., Mancktelow, N., Antognini, M., & Lucchini, R. (2010). Dating of shallow faults: New constraints from the AlpTransit tunnel site (Switzerland). *Geology*, *38*(6), 487–490. https://doi.org/10.1130/G30785.1